Effect of magnetoexciton correlations on the coherent emission of semiconductors

P. Kner, S. Bar-Ad,* M. V. Marquezini,† and D. S. Chemla
Department of Physics, University of California at Berkeley, Berkeley, California 94720
and Materials Sciences Division, Lawrence Berkeley National Laboratory, Berkeley, California 94720

R. Lövenich and W. Schäfer
John von Neumann-Institute for Computing (NIC),‡ Forschungszentrum Jülich, 52425 Jülich, Germany
(Received 21 December 1998)

Mean-field, Hartree-Fock theory has been successful in explaining many nonlinear optical experiments in semiconductors. But recently experiments have shown important cases where the mean-field theory (the semiconductor Bloch equations) fails. One such case is bulk GaAs in a strong magnetic field. Here the exciton-exciton interaction can be tuned by varying the magnetic field, providing an excellent method for studying the transition from a regime where mean-field theory is valid to a regime where exciton-exciton correlations must be taken into account. We perform ultrafast time-resolved four-wave mixing on bulk GaAs in a magnetic field, and compare our experimental results with theoretical calculations which go beyond Hartree-Fock theory. We find excellent qualitative agreement. Furthermore, because of the strong correlations that are present, GaAs in a magnetic field presents an excellent opportunity to study the exciton-exciton correlations themselves. We investigate the coherence of the exciton-exciton correlations as the temperature and free-carrier density are varied, and find a surprising sensitivity of the exciton-exciton correlation coherence to these parameters. [S0163-1829(99)02331-0]

I. INTRODUCTION

Nonlinear spectroscopy of quantum-confined heterostructures has led to the discovery of important effects of many-body interactions on the optical response of semiconductors.[1–4] In most cases the interactions have been treated in a mean-field approximation where the mean-field approximation is made at the two-particle level. Higher-order correlations, beyond the two-particle correlation that leads to the exciton, are neglected. Four-particle correlation effects, such as the bound biexciton resonance are usually treated phenomenologically.[5–7] In the past few years experiments have pointed to failures of the mean-field theory to explain the polarization dependence of the nonlinear optical response,[8–11] pump-probe measurements,[12] and biexciton effects. Theories based on different techniques have been developed to go beyond the mean-field approximation.[13–19]

Recently we have reported on results of experiments done on the lowest-energy excitons in bulk GaAs in high magnetic fields and in a polarization configuration (σ^-/σ^-) where no bound biexciton is formed in the absence of a magnetic field. In these measurements there are strong signatures of exciton-exciton (four-particle) correlations in the continuum of unbound biexciton states.[20,21] We have taken advantage of the strong four-particle correlation signal to investigate the coherence properties of these four-particle correlations, objects rarely accessible to direct measurement.[22] In this longer paper, we report in more detail on that work, provide further experimental evidence for four-particle correlations, and present a detailed treatment of the theory, including results on the effect of the continuum and the equations for treating the presence of an incoherent exciton population. Application of a magnetic field also results in a series of Fano resonances arising from the quantum interference between high-lying excitonic states and lower-energy continua. These resonances have been studied elsewhere.[23–26]

One motivation for this work is to study how magnetic confinement affects the interactions between strongly distorted hydrogenlike systems. A magnetic field confines electrons and holes in the plane perpendicular to the field, so that applying a magnetic field to a bulk sample of GaAs results in a transition from three-dimensional motion of free electrons and holes to one-dimensional motion. This restriction in motion affects the internal structure of the lowest-lying excitons: the Bohr radius contracts $\propto\sqrt{(|B|)}$ in the plane perpendicular to B, and $\propto\ln(|B|)$ in the direction parallel to B.[27] Thus the exciton will develop a quadrupole moment as the magnetic field is increased.[28] These effects are expected to become important at fields $B>B_c$, where B_c is the field strength at which the cyclotron radius equals the zero-field excitonic Bohr radius $\lambda_c=a_0$. For hydrogen, where $B_c\approx10^4$ T such fields are only found at the surface of neutron stars, and thus currently out of reach of experiments. Conversely, for GaAs, $B_c\approx3.5$ T, and the $B\sim B_c$ regime can be easily studied. For magnetic fields $B\ll B_c$, the magnetic field can be treated as a perturbation on the hydrogen problem, and for $B\gg B_c$ the Coulomb interaction is a perturbation on the electronic Landau levels. The structure of the four-particle bound and unbound states also changes significantly as the ratio B/B_c increases from 0.[29] The regime $B\sim B_c$ is interesting both because of the computational difficulty and the changes in the exciton-exciton ground state that occur in this regime. An important experimental advantage of studying magnetic confinement rather than quantum confinement in heterostructures is that all measurements, for varying degrees of confinement, can be made in one high-quality sample of bulk material.

The dynamics of excitons in magnetic fields have been

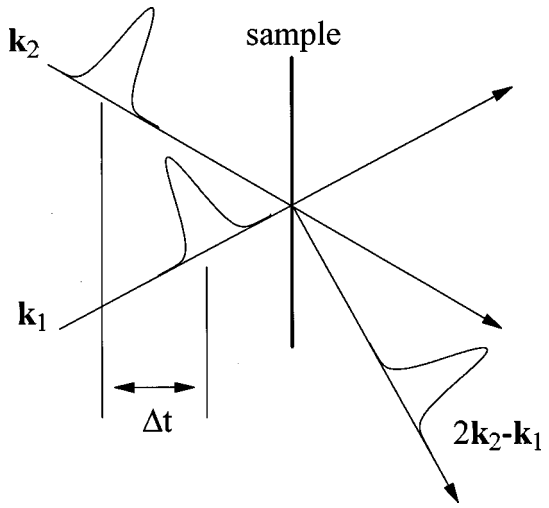

FIG. 1. Four-wave mixing experimental configuration. Two pulses with wave vectors $\vec{k}_1$ and $\vec{k}_2$ are focused on the sample, and the signal emitted in the $2\vec{k}_2-\vec{k}_1$ direction is measured.

studied previously,[30–35] but we believe this is the first study in which strong four-particle correlations have been detected. Two of the previous studies dealt with strongly inhomogeneously broadened systems in which interaction effects are washed out.[32,33] In quantum wells the strong correlation effects we discuss are not seen. A reduction in exciton interactions has been seen for the lowest-lying exciton states in pump-probe measurements.[35] Interactions between the lowest excitons and higher-energy excitons have been measured by a four-wave-mixing measurement, and explained using a multilevel system model.[34] Also, the nonlinear optical response has been calculated within a Hartree-Fock theory.[30] Jiang *et al.*[31] performed a four-wave mixing measurement in the frequency domain on bulk GaAs, and saw an increase in the nonlinear signal with increasing magnetic field which they attributed to reduced exciton diffusion.

II. BACKGROUND

The technique we used to study the exciton interactions was four-wave mixing (FWM). Two pulses of light with frequency ω, resonant with the exciton, and wave vectors $\vec{k}_1$ (pulse 1) and $\vec{k}_2$ (pulse 2), are focused on the sample, separated by a time delay Δt, and the FWM signal is detected in the $2\vec{k}_2-\vec{k}_1$ direction (see Fig. 1). The FWM signal is analyzed in three ways. The total energy in the signal as a function of time delay, Δt, is the time-integrated FWM (TI-FWM). At a given time delay, the signal can be measured in the frequency domain, the FWM power spectrum (FWM-PS), or the time domain, time-resolved FWM (TR-FWM).

For an atomlike multilevel system without interactions, the only nonlinearity is due to Pauli Blocking (PB), and the FWM vanishes for $\Delta t<0$, i.e., pulse 2 arriving first. For $\Delta t>0$, both the TI-FWM and TR-FWM decay with a time constant $T_2/2$, where T_2 is the dephasing time.[36] The FWM-PS is a Lorentzian peak with a width $2\hbar/T_2$. In a model of the semiconductor in which the Coulomb interaction is ignored, the semiconductor is an inhomogeneously broadened set of atomlike two-level systems indexed by the crystal momentum $\vec{k}$.

The next level of approximation is to treat the Coulomb interaction in the time-dependent Hartree-Fock approximation. This leads to the well-known semiconductor Bloch equations (SBE's).[1] These have been used to explain and predict many experimental results in semiconductors, including the ac Stark effect,[1,38] TI- and TR-FWM in quantum wells,[39,40] phase measurements,[3] and photon echoes from the continuum states,[41,42] to name a few.

We will not go into the details of the SBE's which have been discussed in numerous places,[37,40,43] except to emphasize that the SBE's are a mean-field theory by which we mean that the polarization of each exciton only interacts with an effective electric field due to the external applied field and the average polarization field created by all the other excitons. In this case the order parameter is the two-particle density matrix which comprises the polarization and the electron and hole occupations. In the stationary limit, the SBE's share many features with the BCS theory of superconductivity.[1] The SBE's are most frequently used in the relaxation-time approximation, in which processes beyond the Hartree-Fock approximation which contribute to dephasing are approximated by simple exponential decays. The Hartree-Fock approximation does not change quasiparticle lifetimes or dephasing rates. Correlations beyond the two-particle correlation between the electron and hole are not taken into account, so that both bound and unbound biexcitons, which are correlated states of four particles, are not included.

The SBE's were able to explain experiments[2,40] in which a FWM signal was measured for $\Delta t<0$. The Coulomb interaction between electron-hole pairs results in an interaction term between polarizations. This term produces a signal for $\Delta t<0$ which rises twice as fast as the decay, as was seen experimentally. The prediction of a rise time of $T_2/4$ is a very general result of the SBE's, and is not dependent on the details of the excitation or the material, assuming homogeneous broadening. Inhomogeneous broadening in the sample results in a weaker signal for $\Delta t<0$.[44]

Different approximation schemes have been used to extend the SBE's beyond the relaxation time approximation. One well-known scheme is the inclusion of excitation-induced dephasing (EID).[11,45] Here the density dependence of the dephasing is calculated. $\gamma=\gamma_0+\gamma'\Delta n$, where γ' is calculated within the screened Hartree-Fock approximation. The change in dephasing appears in the EID theory at fifth order in the electric field.

EID has been able to explain some experimental results which the SBE's in the relaxation time approximation could not explain. Beyond the simple density dependence of the dephasing, EID has also been able to explain the experimental fact that the strength of the FWM signal in GaAs structures is strongly dependent on the relative polarization of the two beams. EID does not affect the rise time predicted by the SBE's.[46]

Since we are interested in processes requiring a theory beyond the SBE's, it is instructive to know the prediction of that theory. Figure 2 shows a calculation of the SBE's in the relaxation-time approximation for TI-FWM for bulk GaAs in a magnetic field in the same configuration as our experiment (see below and Ref. 20). Here we see the characteristic rise and decay times of $1/4\gamma$ and $1/2\gamma$, where γ is the dephasing rate. There are oscillations in the signal at the frequency of

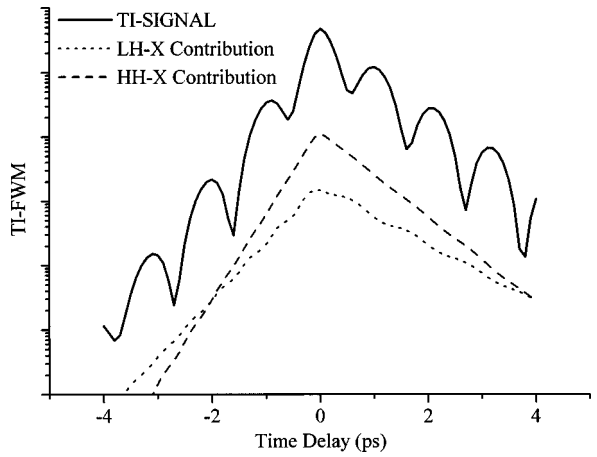

FIG. 2. Calculation of the TI-FWM for bulk GaAs in a magnetic field using the SBE's. The lh-X and hh-X contributions are the area under the lh-X and hh-X emission peaks in the spectrum of the FWM. Note that the rise time is twice as fast as the decay time, and that there are almost no oscillations in the individual lh-X and hh-X contributions.

the energy splitting between the light-hole exciton (lh-X) and the heavy-hole exciton (hh-X). In the configuration of our experiment in which both beams are σ^- polarized, the two excitons do not share a band so there is no PB nonlinearity. There is no Coulomb interaction between them because the matrix element of the Coulomb interaction between these states is zero due to the orthogonality of the spin part of the wave functions.[47] Thus the oscillations in the total signal are polarization interference and not quantum beats, and there are only small oscillations in the signals emitted by the individual excitons. These small oscillations are due to the spectral overlap of the two exciton lines.[48]

III. EXPERIMENTAL SETUP

We performed degenerate four-wave mixing in the self-diffraction configuration (FWM) on a sample of high-quality bulk GaAs in a magnetic field. The excitation pulses were co-circularly polarized (σ^-) 100-fs pulses from a Ti-sapphire laser. The TI-FWM measurements were made by sending the FWM into a GaAs photomultiplier tube. The FWM-PS were taken with a 0.25-m spectrometer and optical multichannel analyzer. And the TR-FWM were made by up-converting the FWM with a reference pulse in a 1-mm BBO crystal.

The samples we studied are 0.25-μm-thick crystals of molecular-beam-epitaxy (MBE) grown GaAs glued to c-axis sapphire substrates and etched for transmission experiments. To avoid any band bending effects, the bulk GaAs layers are sandwiched between two Al_xGaAs_{1-x} layers. In addition, the samples are antireflection coated on both sides. Due to mechanical strain induced by the substrate, the heavy- and light-hole bands are split, resulting in two distinct exciton species (the hh-X and lh-X).[49] The samples are kept in a magneto-optical cryostat, $B=0\rightarrow 12$ T. We studied two samples grown in different MBE machines which we will refer to as sample Nos. 1 and 2.

We have done experiments on samples of different thickness and checked that these samples are optically thin. In optically dense samples, propagation effects can also result in a signal for $\Delta t<0$ with a rise time of $T_2/4$ and nonlinear beating in the TR-FWM and TI-FWM signals.[50,51] More importantly, propagation also leads to reabsorption of the FWM which shows up in the FWM-PS as a dip in resonance peaks. We see reabsorption effects in samples with thickness 0.5 and 1 μm, but not in the 0.25-μm samples which were selected for our experiments.

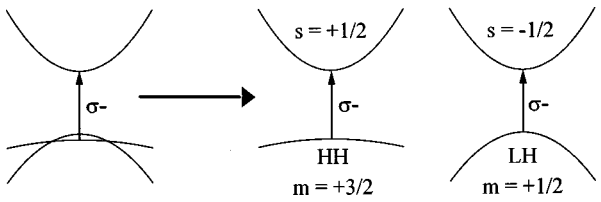

FIG. 3. Schematic band diagram of bulk GaAs, showing the σ^- optical transitions. The degeneracy of the lh and hh bands at $k=0$ has been lifted by stress. Band mixing has not been taken into account.

The cocircular polarization configuration was chosen to minimize the effect of bound biexcitons on the FWM response. In this configuration hh-X/hh-X and lh-X/lh-X singlet states (the bound state at $B=0$ T) cannot be formed because the lh-X electrons all have the same spin ($s=-\frac{1}{2}$) as do the hh-X electrons ($s=+\frac{1}{2}$). In the exciton basis, to lowest order, there is no interaction term between the lh-X and hh-X[52] so the attractive interaction leading to bound lh-X/hh-X states is weak and their oscillator strength is small. We do not consider them in our analysis. Figure 3 shows the band structure, emphasizing the fact that the lh and hh transitions do not share a conduction band in this configuration. For the majority of the measurements, we have kept $I_{k_1}\approx I_{k_2}$ in order to keep the excitation density roughly constant as Δt is varied. And we have kept $T=1.6$ K to avoid dephasing due to phonons. Also for most of the measurements, the laser was tuned so that its center frequency was approximately between the lh-X and the hh-X. As B was varied, the laser was tuned to keep the overlap the same, keeping the excited exciton density roughly constant. These were the experimental conditions except for measurements at $B=10$ T, where we varied the temperature and the laser detuning (Sec. VII).

IV. EXPERIMENTAL RESULTS

We begin discussing the experimental results by examining the linear spectra. Linear absorption spectra of the GaAs sample are shown in Fig. 4 for a few different magnetic-field strengths applied perpendicular to the plane of the sample. The lowest-lying resonances are the Lorentzian magneto-excitons which are under study in this paper. While there is a diamagnetic shift of the excitons as B is changed from 0 to 10 T, the changes in the oscillator strength and linewidth are small. The measurements were made with a light bulb, so the excitation density is extremely low. Both the lh-X and hh-X can be fit fairly well with Lorentzians. At 0 T, for the lh-X, $\Gamma_{\mathrm{FWHM}}=2\gamma_{lh}=0.35$ meV, and for the hh-X, $2\gamma_{hh}=0.48$ meV. At 10 T, $2\gamma_{lh}=0.36$ meV, and $2\gamma_{hh}=0.31$ meV. In addition we have made photoluminescence measurements on these samples to verify that the impurity concentration is

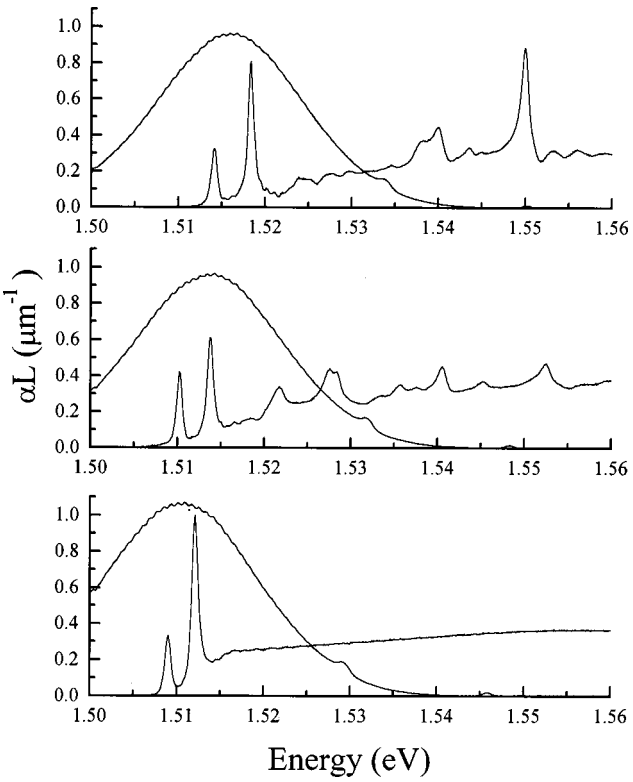

FIG. 4. Linear absorption of the 0.25-μm sample of GaAs at $B=0$, 6, and 10 T. Typical laser spectra for the measurements are also shown. For each measurement, the laser is tuned to resonance with lh-X and hh-X.

low. From the linear spectra we then expect a decay time of $T_2/2=\hbar/2\gamma\approx 1.65$ps for the TI-FWM.

Figure 5 shows a series of TI-FWM measurements on sample No. 1 for different magnetic-field strengths. The TI-FWM at $B=0$ T has an exponential decay with oscillations for $\Delta t>0$. The decay time, τ_d, is 1.48 ps, in reasonable agreement with the linewidths of the linear spectra. Of course, the density, $N\approx 5\times 10^{15}\,\mathrm{cm}^{-3}$, is much higher than the density excited in the linear measurements, so the decay time is shorter. The oscillation period corresponds to the lh-X/hh-X energy splitting. For $\Delta t<0$, there is a much smaller signal with a rise time, τ_r, of 0.25 ps. This signal—which does not follow the rise of the laser pulse—is clear evidence of exciton-exciton interactions. There is also a large fast signal around $\Delta t=0$, the coherent peak. The decay of the signal for $\Delta t>0$ gives the exciton dephasing time. The $\Delta t<0$ signal is a result of the Coulomb interaction between the excitons and is in reasonable agreement with the SBE's. The fact that the rise time is not twice as fast as the decay time is most likely due to the influence of excited and continuum states with faster dephasing times. A small inhomogeneous broadening in the sample might also contribute to the faster rise time. The oscillations are quantum beats between the lh-X and hh-X,[53] which will be conclusively demonstrated with the FWM-PS and the TR-FWM data later in the paper.

As the magnetic field is increased, the positive time signal, $S_{TI}^{+}\equiv S_{TI}(\Delta t>0)$, changes only slightly: τ_d remains about 1.5 ps while the signal magnitude increases slightly and the depth of the quantum beats diminishes. But qualitatively, the signal does not change. τ_d is determined by a fit of

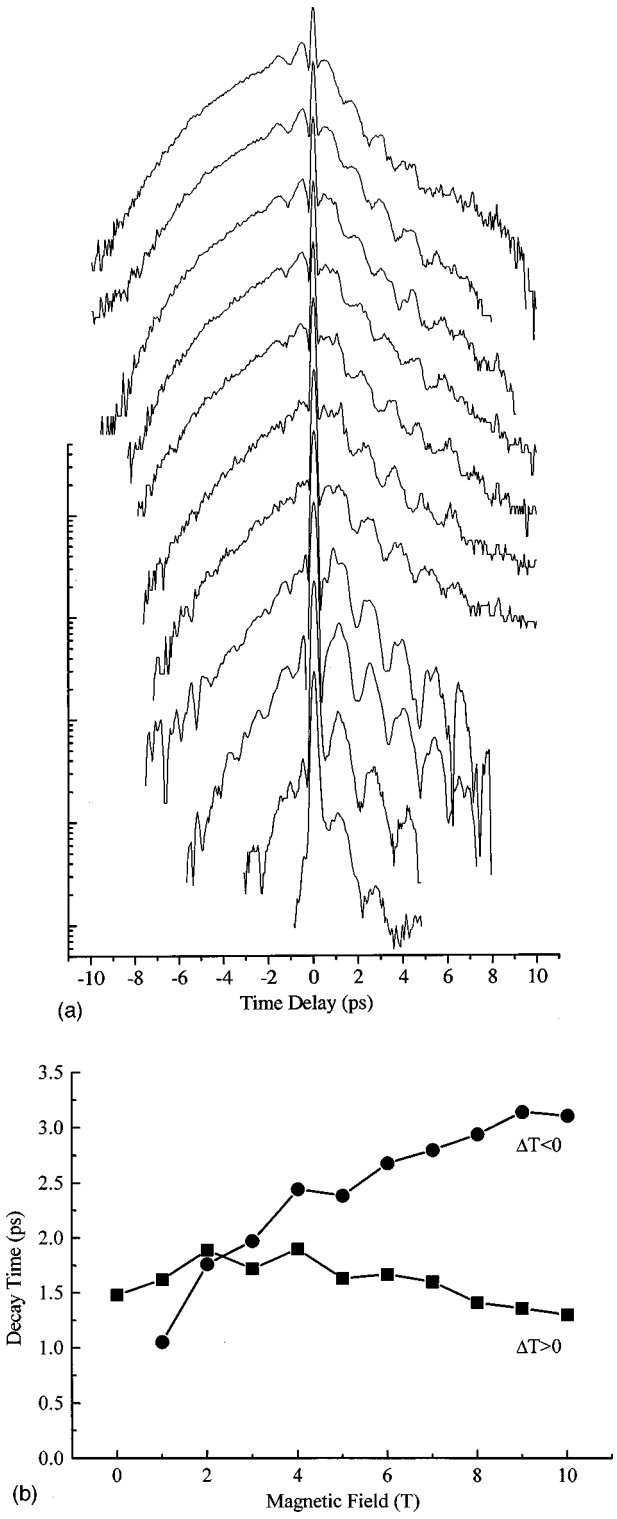

FIG. 5. (a) TI-FWM on sample No. 1 for magnetic fields from 0 (bottom) to 10 (top) T every 1 T. The curves are plotted on a logarithmic scale and displaced for clarity. For these measurements, $N\approx 5\times 10^{15}\,\mathrm{cm}^{-3}$. (b) τ_r and τ_d vs B. As the magnetic field is increased, S_{TI}^{-} increases while there are only minor changes in S_{TI}^{+}.

S_{TI}^{+} to $Ae^{-\Delta t/\tau_d}[1+C\cos(\omega\Delta t+\phi)]$.

The negative time signal $S_{TI}^{-}\equiv S_{TI}(\Delta t<0)$, on the other hand, changes drastically as the magnetic field is increased. The magnitude of the signal changes by more than two orders of magnitude at $\Delta t=-500$ fs. In contrast, at $\Delta t=0$, the

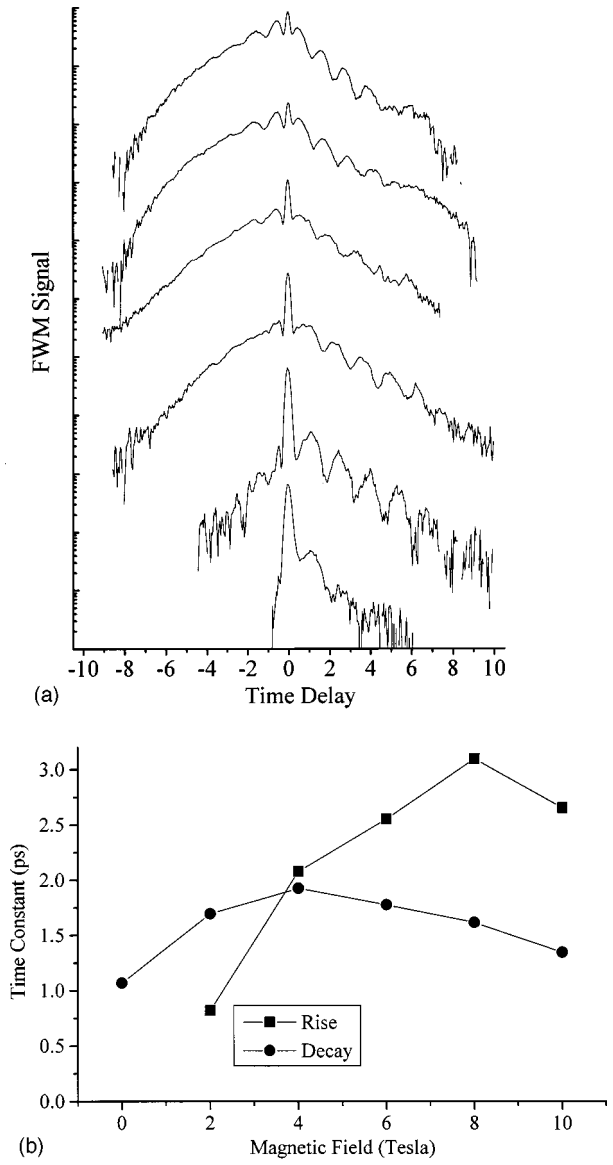

FIG. 6. (a) TI-FWM vs B on sample No. 2 for magnetic fields from 0 T (bottom) to 10 T (top) every 2 T. (b) τ_r and τ_d vs B.$N \approx 10^{16}\,\mathrm{cm}^{-3}$. Sample No. 2 shows the same behavior with magnetic field as sample No. 1 demonstrating that the effect is not sample dependent.

change is only about a factor of 4. τ_r goes from 0.25 to 3.0 ps. We have estimated τ_r with a simple exponential fit to the negative time signal for $-0.4 > \Delta t > -5$ ps. Clearly, the rise of the signal is not a simple exponential, which suggests that non-Markovian processes are important. From the slow rise time of the TI-FWM ($\gg 1/4\gamma$) it is evident that, at high magnetic field, effects that are not included in the SBE's become important. The rise and decay times of the TI-FWM vs B are plotted in Fig. 5(b), showing that above about 4 T, τ_r becomes greater than τ_d. It is interesting to compare this value with $B_c \approx 3.5$ T.

Figure 6 shows the measurements from sample No. 2. We see exactly the same behavior on the second sample as we do on sample No. 1. The rise and decay times for the samples are quite similar. This, and the narrow linewidths of both samples, indicate that both samples are high quality, and that the effects we are measuring are intrinsic and not sample

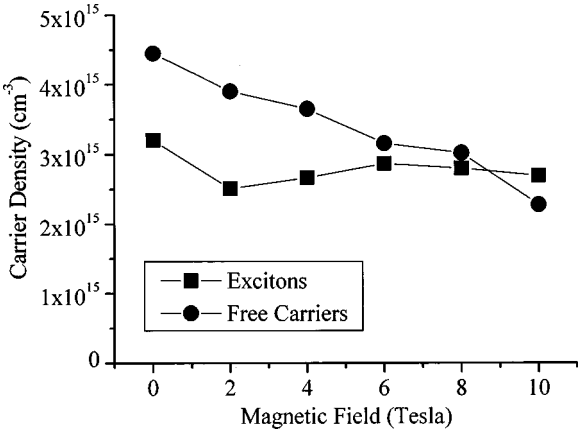

FIG. 7. The number of excitons and free e-h pairs excited by one pulse vs magnetic field. This plot corresponds to the measurement in Fig. 5. As the magnetic field is increased, the number of excited excitons remains roughly constant, whereas the number of excited free carriers decreases.

dependent. The differences in dephasing time between the two samples are partly due to different excitation density and partly due to the larger linewidth of sample No. 2. At $B = 0$ T, from the linear spectra for sample No. 2, $2\gamma_{lh} = 0.58$ meV and $2\gamma_{hh} = 0.53$ meV. The excitation densities for the measurements on sample No. 2 are roughly 1.6 times higher than for sample No. 1.

We have calculated the density of excited excitons and excited free carriers from the measured laser spectra and the measured absorption spectra. The calculated densities for sample No. 1 are shown in Fig. 7. Due to the change in the continuum absorption, the number of free carriers excited decreases as the magnetic field is increased although the laser is tuned to keep the number of excitons excited roughly constant. Thus, at high magnetic fields, there are fewer free carriers available to screen the Coulomb interaction, and the interactions between the excitons are stronger. This agrees with the experimental result that S_{TI}^{-}, which is due to interactions, grows with B.The increase in the strength of the Coulomb interaction cannot fully explain the change in S_{TI}^{-} with B because S_{TI}^{-} does not simply grow with B but also changes qualitatively.

The results of TR-FWM and FWM-PS measurements are also in clear contradiction to the predictions of the SBE's. A series of TR-FWM measurements at different Δt are shown in Fig. 8. The inset is the corresponding TI-FWM. There are very pronounced beats in the TR-FWM for all Δt, consistent with the FWM-PS which shows two peaks, even though the S_{TI}^{-} is smooth. In fact the oscillations in the S_{TI}^{+} are also not very pronounced. In SBE calculations, there are beats in the TI-FWM corresponding to the beats in the TR-FWM. The delayed rise in the TR-FWM is due to interaction effects which have been explained within the framework of the SBE's.[39]

The TR-FWM also provides unambiguous evidence that the sample is homogeneously broadened, and we are looking at a free-induction decay and not a photon echo. If we plot the TR-FWM maximum vs Δt (Fig. 9), for $\Delta t > 0$, the emission time does not increase with Δt. (The fluctuations in peak position are due to changes in the TR-FWM signal

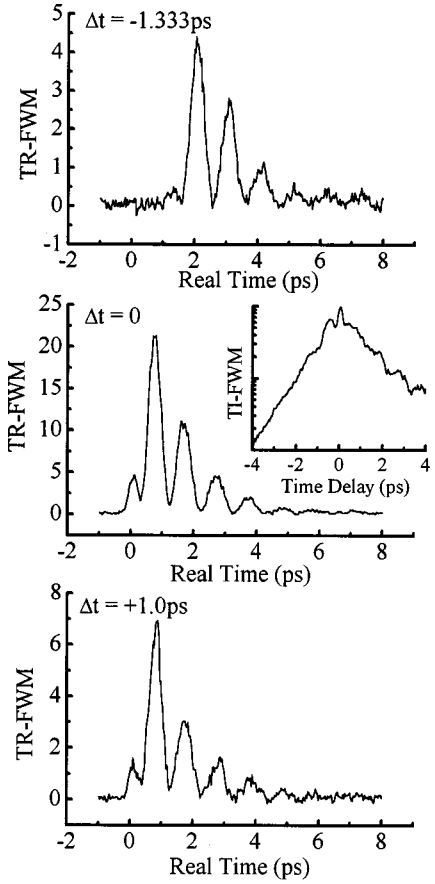

FIG. 8. TR-FWM at $B=10$ T. The inset is the corresponding TI-FWM. Clear oscillations are seen at all delays in the TR-FWM, but, in the TI-FWM, oscillations are only seen for $\Delta t>0$. For these measurements $I_{k_2}\approx 4I_{k_1}$ and $N\approx 10^{16}\,\mathrm{cm}^{-3}$.

which make it difficult to identify the arrival time.) For $\Delta t<0$ the emission time increases in direct proportion to Δt, i.e., the slope of the line is 1, not 2 as it would be for a photon echo. Thus the TR-FWM is emitted immediately after the second pulse as a free-induction decay.

The SBE predict that the lh-X signal is smaller than the hh-X signal because of the smaller oscillator strength of the lh-X. If we look at the FWM-PS at $\Delta t=0$ as a function of magnetic field, we also see the transition from a regime at low-magnetic field consistent with the mean-field theory (at 0 T the lh-X signal is about a factor of 3.5 smaller than the hh-X signal) to a regime at high magnetic field where the lh-X signal is stronger than the hh-X signal. This is shown in Fig. 10.

Within the SBE's (Fig. 2) the beating between the lh-X and hh-X is polarization interference, but the oscillations in our data are quantum beats. The emission of the TR-FWM as a free-induction decay (Fig. 9) is evidence that the beating is quantum beating.[53] The quantum beats can also clearly be seen as a function of Δt at the lh-X and hh-X resonances in a plot of the FWM-PS vs Δt (Fig. 11). As a last piece of spectrally resolved data, Fig. 12 shows a set of FWM-PS at different time delays showing clearly that the relative strength of the lh-X and hh-X signals changes as a function of Δt. This is further evidence of the strong interaction between the lh-X and hh-X which is beyond the mean-field predictions.

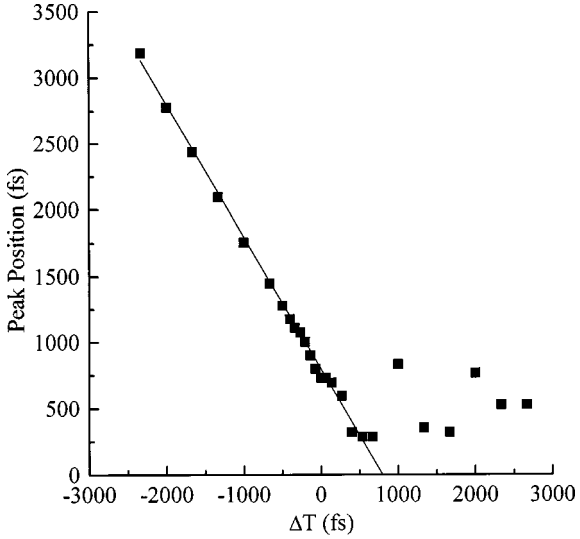

FIG. 9. The time of the TR-FWM maximum vs Δt. The solid line has a slope of 1. This indicates that the FWM signal is emitted immediately after the second pulse which proves both that the excitons are homogeneously broadened and that the oscillations are quantum beats.

V. THEORY

The shape of S_{TI}^{-}, the relative size of the lh-X and hh-X signals, the quantum beats and the exchange of oscillator strength between the lh-X and hh-X with Δt at high magnetic field all cannot be explained by the SBE's. To explain these results, we have to go beyond the mean-field theory. We do this in a systematic way by employing the coherently controlled truncation scheme (CCTS),[54] which was proposed in Ref. 55 and worked out in detail in Refs. 16 and 56. This

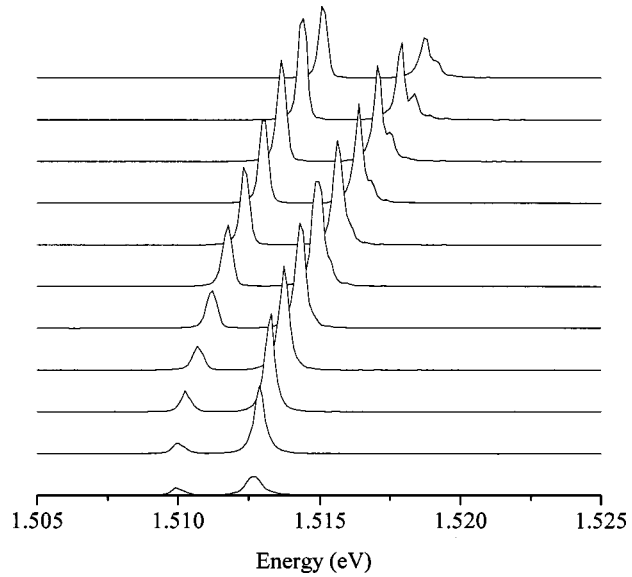

FIG. 10. FWM-PS at $\Delta t=0$ vs. B. These measurements correspond to the TI-FWM from Fig. 5. As the magnetic field is increased, the strength of the lh-X emission relative to the hh-X emission increases, indicating a transition from a regime in agreement with the SBE's to a regime, at high magnetic field, where the SBE's fail.

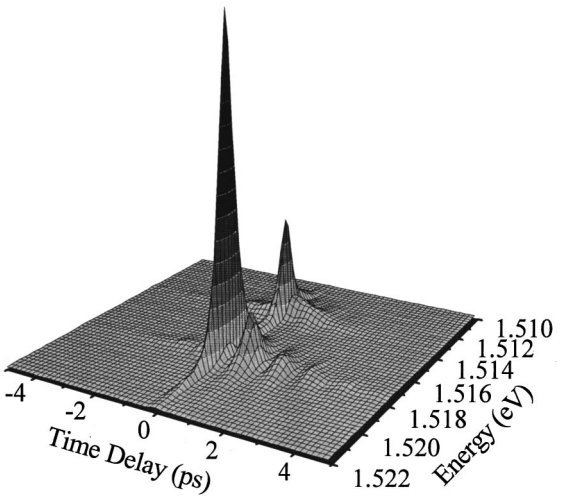

FIG. 11. FWM-PS vs Δt at $B=10$ T. $N\approx 5\times 10^{16}\,\mathrm{cm}^{-3}$. Here quantum beats can clearly be seen on the hh-X emission.

theory was motivated by the properties of coherently driven electron-hole pairs, which are realized for off-resonant excitation conditions in the optical Stark effect, and offers an elegant method to introduce coherent exciton-exciton correlations. In this formalism, when calculating the optical response of the semiconductor at a given order in the laser field, one only retains a finite number of correlation functions of electrons and holes that contribute to that order. This is possible because, in an intrinsic semiconductor initially in the ground state, each e-h pair is created by one photon. Therefore, higher-order correlation functions are proportional to higher powers of the exciting laser electric field and only contribute to higher-order nonlinearities. Although this approach is exact in the ideal, but unrealistic, coherent limit where there are absolutely no dephasing processes, any scattering, producing incoherent contributions to the particle distribution functions, destroys this property. Effects associated with bound biexcitons are automatically included in the CCTS theory.

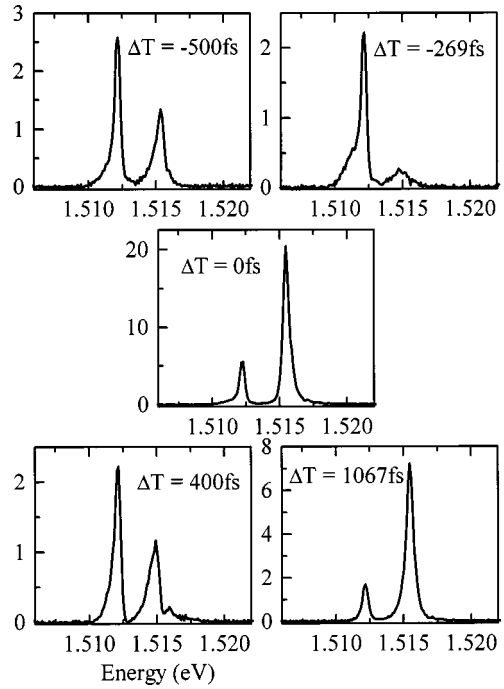

FIG. 12. FWM-PS for different Δt at $B=6$T. There is an exchange of signal strength between the lh-X and hh-X with time delay that is beyond the predictions of the SBE's. $I_{k_2}\approx 4I_{k_1}$. $N\approx 5\times 10^{15}\,\mathrm{cm}^{-3}$.

The CCTS has been successfully applied to FWM and pump-probe experiments that cannot be explained by the SBE's.[10,12,52,57] In particular, the CCTS explains the polarization dependence of the FWM signal, and should be contrasted with phenomenological multi-level models that have been proposed to describe this dependence, but that are not derived rigorously from the semiconductor Hamiltonian.[5,6,58] EID is included in the CCTS via the interference due to the coupling to the biexcitonic continuum. The importance of this coupling has also been emphasized in a recent paper.[59] It is also responsible for antibound states recently observed in ZnSe quantum wells.[60] The CCTS limited to third-order processes in the laser field, is known as the $\chi^{(3)}$-truncation scheme. Although the structure of the theory is well known, the very special aspects of the Coulomb interaction in a magnetic field produce specific features that deserve a discussion. Furthermore, we will comment on an important extension of the $\chi^{(3)}$-truncation scheme to account for incoherent processes. Our starting point is the Hamiltonian of electrons and holes in the lowest Landau-level, coupled by the dipole-matrix element $\boldsymbol{\mu}_{\mathbf{k}}^{eh}$ to the external laser fields $\mathbf{E}$.

$$
\begin{aligned}
H=&\sum_{\mathbf{k}e}\varepsilon_{\mathbf{k}}^{e}\hat{e}_{\mathbf{k}}^{\dagger}\hat{e}_{\mathbf{k}}+\sum_{\mathbf{k}h}\varepsilon_{\mathbf{k}}^{h}\hat{h}_{\mathbf{k}}^{\dagger}\hat{h}_{\mathbf{k}}+\sum_{\mathbf{k}eh}(\boldsymbol{\mu}_{\mathbf{k}}^{eh}\mathbf{E}\hat{e}_{\mathbf{k}}^{\dagger}\hat{h}_{\mathbf{k}}^{\dagger}+\boldsymbol{\mu}_{\mathbf{k}}^{he}\mathbf{E}\hat{h}_{\mathbf{k}}\hat{e}_{\mathbf{k}})\\
&+\frac{1}{2}\sum_{\mathbf{k}\mathbf{k}'\mathbf{q}}\left\{v_{\mathbf{q}}^{k_y-k_y'+q_y}\left[\sum_{ee'}\hat{e}_{\mathbf{k}+\mathbf{q}}^{\dagger}\hat{e}_{\mathbf{k}'-\mathbf{q}}^{\dagger}\hat{e}_{\mathbf{k}'}\hat{e}_{\mathbf{k}}\right.\right.\\
&\left.+\sum_{hh'}\hat{h}_{\mathbf{k}+\mathbf{q}}^{\dagger}\hat{h}_{\mathbf{k}'-\mathbf{q}}^{\dagger}\hat{h}_{\mathbf{k}'}\hat{h}_{\mathbf{k}}\right]-v_{\mathbf{q}}^{k_y-k_y'}\sum_{eh}[\hat{e}_{\mathbf{k}+\mathbf{q}}^{\dagger}\hat{h}_{\mathbf{k}'-\mathbf{q}}^{\dagger}\hat{h}_{\mathbf{k}'}\hat{e}_{\mathbf{k}}\\
&\left.+\hat{h}_{\mathbf{k}+\mathbf{q}}^{\dagger}\hat{e}_{\mathbf{k}'-\mathbf{q}}^{\dagger}\hat{e}_{\mathbf{k}'}\hat{h}_{\mathbf{k}}]\right\}. \qquad (1)
\end{aligned}
$$

The single-particle energies are given by

$$\varepsilon_{\mathbf{k}}^{e,h}=\varepsilon_{0}^{e,h}+\frac{\hbar^2}{2m_{e,h}l^2}+\frac{\hbar^2k_z^2}{2m_{e,h}}, \qquad (2)$$

where l is the magnetic length, $l=\sqrt{\hbar/eB}$, and k_z is the momentum along the direction $\|\vec{B}$. For electrons and holes in the lowest Landau level, the Coulomb interaction in the Landau gauge is given by

$$v_{\mathbf{q}}^{k_y}=\frac{e^2}{2\pi\varepsilon_0 L^2}\int_{-\infty}^{\infty}dq_x\frac{e^{-l^2(q_x^2+q_y^2)/2}}{q_x^2+\mathbf{q}^2}e^{il^2k_yq_x}, \qquad (3)$$

and $\hat{e}_{\mathbf{k}}^{\dagger}$ and $\hat{h}_{\mathbf{k}}^{\dagger}$ are the Fermi operators for electrons and holes, with two-dimensional $\mathbf{k}$ vectors in the k_y-k_z plane. The optical properties are determined by the polarization $\vec{P}=\Sigma_{ehk}\vec{\mu}_{eh}P_k^{eh}$, where $P_{\mathbf{k}}^{eh}=\langle\hat{e}_{\mathbf{k}}^{\dagger}\hat{h}_{-\mathbf{k}}^{\dagger}\rangle$, is the transition amplitude between an electron in band e and a hole in band h with respective wavevectors k and $-k$. $P_{\mathbf{k}}^{eh}$ obeys the equation

$$\left(-i\hbar\frac{\partial}{\partial t}-\varepsilon^{e}_{\mathbf{k}}-\varepsilon^{h}_{\mathbf{k}}-i\hbar\gamma_P\right)P^{eh}_{\mathbf{k}}+\sum_{\mathbf{q}}\nu^{0}_{\mathbf{q}}P^{eh}_{\mathbf{k}+\mathbf{q}}$$
$$=\sum_{h'}\boldsymbol{\mu}^{h'e}_{\mathbf{k}}\mathbf{E}(\delta_{h,h'}-f^{hh'}_{\mathbf{k}})-\sum_{e'}\boldsymbol{\mu}^{he'}_{\mathbf{k}}\mathbf{E}f^{e'}_{\mathbf{k}}+\frac{\partial}{\partial t}P^{eh}_{\mathbf{k}}\Big|_{int}, \tag{4}$$

where the interaction contribution is given by

$$\frac{\partial}{\partial t}P^{eh}_{\mathbf{k}}\Big|_{int}=\sum_{\mathbf{k}'\mathbf{q}}v^{k_y-k'_y}_{\mathbf{q}}\Big\{\sum_{e'}[\langle\hat{e}^{\dagger}_{\mathbf{k}+\mathbf{q}}\hat{h}^{\dagger}_{-\mathbf{k}}\hat{e}^{\dagger}_{\mathbf{k}'}\hat{e}_{\mathbf{k}'+\mathbf{q}}\rangle$$
$$-\langle\hat{e}^{\dagger}_{\mathbf{k}}\hat{h}^{\dagger}_{-\mathbf{k}-\mathbf{q}}\hat{e}^{\dagger}_{\mathbf{k}'+\mathbf{q}}\hat{e}_{\mathbf{k}'}\rangle]$$
$$+\sum_{h'}[\langle\hat{e}^{\dagger}_{\mathbf{k}}\hat{h}^{\dagger}_{-\mathbf{k}-\mathbf{q}}\hat{h}^{\dagger}_{-\mathbf{k}'}\hat{h}_{-\mathbf{k}'-\mathbf{q}}\rangle$$
$$-\langle\hat{e}^{\dagger}_{\mathbf{k}+\mathbf{q}}\hat{h}^{\dagger}_{-\mathbf{k}}\hat{h}^{\dagger}_{-\mathbf{k}'-\mathbf{q}}\hat{h}_{-\mathbf{k}'}\rangle]\Big\}. \tag{5}$$

Within the $\chi^{(3)}$-truncation scheme we make use of particle-number conservation, which allows the introduction, in Eq. (5), of six-point instead of four-point correlation functions according to the relation

$$\langle\hat{e}^{\dagger}_{\mathbf{k}_1}\hat{h}^{\dagger}_{\mathbf{k}_2}\hat{e}_{\mathbf{k}_3}\hat{e}_{\mathbf{k}_4}\rangle=\sum_{\mathbf{k},h'}\langle\hat{e}^{\dagger}_{\mathbf{k}_1}\hat{h}^{\dagger}_{\mathbf{k}_2}\hat{e}_{\mathbf{k}_3}\hat{h}'^{\dagger}_{\mathbf{k}}\hat{h}'_{\mathbf{k}}\hat{e}_{\mathbf{k}_4}\rangle$$
$$-\sum_{\mathbf{k},e'}\langle\hat{e}^{\dagger}_{\mathbf{k}_1}\hat{h}^{\dagger}_{\mathbf{k}_2}\hat{e}_{\mathbf{k}_3}\hat{e}'^{\dagger}_{\mathbf{k}}\hat{e}'_{\mathbf{k}}\hat{e}_{\mathbf{k}_4}\rangle. \tag{6}$$

The second contribution on the right-hand side of Eq. (6) is at least fifth order in the excitation field and neglected at the $\chi^{(3)}$ level. The resulting six-point functions are factorized into all possible products of two-point and four-point functions. This procedure allows us to split the interaction contribution [Eq. (5)], into a Hartree-Fock contribution and a correlation contribution. The Hartree-Fock contribution is

$$\frac{\partial}{\partial t}P^{eh}_{\mathbf{k}}\Big|_{HF}=\sum_{\mathbf{q},e'h'}v^{0}_{\mathbf{k}-\mathbf{q}}[P^{eh'}_{\mathbf{q}}f^{h'h}_{\mathbf{k}}\delta_{e,e'}+P^{e'h}_{\mathbf{q}}f^{ee'}_{\mathbf{k}}\delta_{h,h'}$$
$$-P^{e'h}_{\mathbf{k}}f^{ee'}_{\mathbf{q}}\delta_{h,h'}-P^{eh'}_{\mathbf{k}}f^{h'h}_{\mathbf{q}}\delta_{e,e'}]. \tag{7}$$

The one-particle distribution function is the sum of a coherent and an incoherent contribution

$$f^{ee'}_{\mathbf{k}}=\sum_{h'}P^{eh'}_{\mathbf{k}}P^{eh'*}_{\mathbf{k}}+\sum_{\mathbf{q},h'}N^{eh'e'h'}_{\mathbf{k},\mathbf{q},\mathbf{k},\mathbf{q}}, \tag{8}$$

where we introduce the pair-density correlation function

$$N^{ehe'h'}_{\mathbf{k}_1,\mathbf{k}_2,\mathbf{k}_3,\mathbf{k}_4}=\langle\hat{e}^{\dagger}_{\mathbf{k}_1}\hat{h}^{\dagger}_{\mathbf{k}_2}\hat{e}'_{\mathbf{k}_3}\hat{h}'_{\mathbf{k}_4}\rangle-\langle\hat{e}^{\dagger}_{\mathbf{k}_1}\hat{h}^{\dagger}_{\mathbf{k}_2}\rangle\langle\hat{e}'_{\mathbf{k}_3}\hat{h}'_{\mathbf{k}_4}\rangle, \tag{9}$$

which determines the incoherent part of the one-particle distribution function. The correlation contribution to Eq. (5) consists of two parts. One is incoherent, and determined by the pair-density correlation function $N^{ehe'h'}_{\mathbf{k}_1,\mathbf{k}_2,\mathbf{k}_3,\mathbf{k}_4}$, and the second one is due to the biexcitonic correlation function

$$B^{ehe'h'}_{\mathbf{k}_1,\mathbf{k}_2,\mathbf{k}_3,\mathbf{k}_4}=\langle\hat{e}^{\dagger}_{\mathbf{k}_1}\hat{h}^{\dagger}_{\mathbf{k}_2}\hat{e}'^{\dagger}_{\mathbf{k}_3}\hat{h}'^{\dagger}_{\mathbf{k}_4}\rangle$$
$$-\langle\hat{e}^{\dagger}_{\mathbf{k}_1}\hat{h}^{\dagger}_{\mathbf{k}_2}\rangle\langle\hat{e}'^{\dagger}_{\mathbf{k}_3}\hat{h}'^{\dagger}_{\mathbf{k}_4}\rangle+\langle\hat{e}^{\dagger}_{\mathbf{k}_1}\hat{h}^{\dagger}_{\mathbf{k}_4}\rangle\langle\hat{e}'^{\dagger}_{\mathbf{k}_3}\hat{h}^{\dagger}_{\mathbf{k}_2}\rangle. \tag{10}$$

This correlation function has a very straightforward interpretation. The operators in the first term of Eq. (10) create two e-h pairs, and thus $B^{ehe'h'}_{\mathbf{k}_1,\mathbf{k}_2,\mathbf{k}_3,\mathbf{k}_4}$ corresponds to a two photon transition for excitation at the band edge. Two factorized terms are subtracted off the first term, and correspond to uncorrelated creation of the two e-h pairs, including the sign change in front of the third term that results from the rearrangement of the Fermi operators. Therefore, $B^{ehe'h'}_{\mathbf{k}_1,\mathbf{k}_2,\mathbf{k}_3,\mathbf{k}_4}$ represents the coherent part of the two photon transition and vanishes if the generated excitons are not coherent with each other. When all these elements are collected, the correlation contribution to Eq. (5) takes the form

$$\frac{\partial}{\partial t}P^{eh}_{\mathbf{k}}\Big|_{\mathrm{corr}}=\sum_{\mathbf{k}'\mathbf{q},e'h'}v^{k_y-k'_y}_{\mathbf{q}}\{[P^{e'h'*}_{\mathbf{k}'}-P^{e'h'*}_{\mathbf{k}'+\mathbf{q}}][B^{ehe'h'}_{\mathbf{k}+\mathbf{q},\mathbf{k},\mathbf{k}',\mathbf{k}'+\mathbf{q}}$$
$$+B^{ehe'h'}_{\mathbf{k},\mathbf{k}+\mathbf{q},\mathbf{k}'+\mathbf{q},\mathbf{k}'}]+P^{e'h}_{\mathbf{k}}N^{e'h'eh'}_{\mathbf{k},\mathbf{k}',\mathbf{k}+\mathbf{q},\mathbf{k}'+\mathbf{q}}$$
$$-P^{e'h}_{\mathbf{k}+\mathbf{q}}N^{e'h'eh'}_{\mathbf{k}+\mathbf{q},\mathbf{k}'+\mathbf{q},\mathbf{k},\mathbf{k}'}+P^{eh'}_{\mathbf{k}}N^{e'h'e'h}_{\mathbf{k}'+\mathbf{q},\mathbf{k},\mathbf{k}',\mathbf{k}+\mathbf{q}}$$
$$-P^{eh'}_{\mathbf{k}+\mathbf{q}}N^{e'h'e'h}_{\mathbf{k}'+\mathbf{q},\mathbf{k}+\mathbf{q},\mathbf{k}',\mathbf{k}}+[P^{e'h'}_{\mathbf{k}'}-P^{e'h'}_{\mathbf{k}'+\mathbf{q}}]$$
$$\times[N^{ehe'h'}_{\mathbf{k}'+\mathbf{q},\mathbf{k}',\mathbf{k}+\mathbf{q},\mathbf{k}}+N^{ehe'h'}_{\mathbf{k}',\mathbf{k}'+\mathbf{q},\mathbf{k},\mathbf{k}+\mathbf{q}}]\}. \tag{11}$$

The biexcitonic correlation function contributes to the linear dephasing of the polarization in contrast to Green's-functions theory, as shown already in Ref. 52. The equation of motion of the pair-density correlation function has the form

$$\left(-i\hbar\frac{\partial}{\partial t}-\varepsilon^{e}_{\mathbf{k}_1}-\varepsilon^{h}_{\mathbf{k}_2}+\varepsilon^{e'}_{\mathbf{k}_3}+\varepsilon^{h'}_{\mathbf{k}_4}\right)N^{ehe'h'}_{\mathbf{k}_1,\mathbf{k}_2,\mathbf{k}_3,\mathbf{k}_4}$$
$$-\sum_{\mathbf{q}}\nu^{0}_{\mathbf{q}}(N^{ehe'h'}_{\mathbf{k}_1+\mathbf{q},\mathbf{k}_2+\mathbf{q},\mathbf{k}_3,\mathbf{k}_4}-N^{ehe'h'}_{\mathbf{k}_1,\mathbf{k}_2,\mathbf{k}_3+\mathbf{q},\mathbf{k}_4+\mathbf{q}})$$
$$=\frac{\partial}{\partial t}N^{ehe'h'}_{\mathbf{k}_1,\mathbf{k}_2,\mathbf{k}_3,\mathbf{k}_4}\Big|_{\mathrm{source}}+\frac{\partial}{\partial t}N^{ehe'h'}_{\mathbf{k}_1,\mathbf{k}_2,\mathbf{k}_3,\mathbf{k}_4}\Big|_{\mathrm{scatt}}. \tag{12}$$

In its simplest version the source term is proportional to $\gamma_P P^{eh}_{\mathbf{k}_1}P^{e'h'*}_{\mathbf{k}_3}\delta_{\mathbf{k}_1,\mathbf{k}_2}\delta_{\mathbf{k}_3,\mathbf{k}_4}$, i.e., the decay of the coherent polarization. The scattering contribution drives the pair-density correlation function toward its quasi-equilibrium value. In principle a $\chi^{(3)}$-truncation theory cannot account for these processes. Since this is an incoherent contribution to the dynamics, the CCTS is not well suited, and one should refer to other methods of many-particle theory. If the Coulomb potential is treated perturbatively, one can reduce these incoherent dephasing contributions in Eq. (4) in the Markovian approximation to the result known from nonequilibrium Green's-functions theory.[61,62]

The equation of motion of the biexciton correlation function is

$$\left(-i\hbar\frac{\partial}{\partial t}-\varepsilon^{e}_{\mathbf{k}+\mathbf{q}}-\varepsilon^{h'}_{\mathbf{k}'+\mathbf{q}}-\varepsilon^{e'}_{\mathbf{k}'}-\varepsilon^{h}_{\mathbf{k}}-i\gamma_B\right)B^{ehe'h'}_{\mathbf{k}+\mathbf{q},\mathbf{k},\mathbf{k}',\mathbf{k}'+\mathbf{q}}-\sum_{\mathbf{q}'}\,[v^{k_y-k'_y+q'_y-q_y}_{\mathbf{q}'}B^{ehe'h'}_{\mathbf{k}+\mathbf{q}+\mathbf{q}',\mathbf{k},\mathbf{k}'-\mathbf{q}',\mathbf{k}'+\mathbf{q}}$$
$$+v^{k'_y-k_y+q'_y-q_y}_{\mathbf{q}'}B^{ehe'h'}_{\mathbf{k}+\mathbf{q},\mathbf{k}+\mathbf{q}',\mathbf{k}',\mathbf{k}'+\mathbf{q}-\mathbf{q}'}-v^{k_y-k'_y}_{\mathbf{q}'}B^{ehe'h'}_{\mathbf{k}+\mathbf{q}+\mathbf{q}',\mathbf{k}+\mathbf{q}',\mathbf{k}',\mathbf{k}'+\mathbf{q}}-v^{k'_y-k_y}_{\mathbf{q}'}B^{ehe'h'}_{\mathbf{k}+\mathbf{q},\mathbf{k},\mathbf{k}'+\mathbf{q}',\mathbf{k}'+\mathbf{q}+\mathbf{q}'}$$
$$-v^{q_y}_{\mathbf{q}'}B^{ehe'h'}_{\mathbf{k}+\mathbf{q}+\mathbf{q}',\mathbf{k},\mathbf{k}',\mathbf{k}'+\mathbf{q}+\mathbf{q}'}-v^{-q_y}_{\mathbf{q}'}B^{ehe'h'}_{\mathbf{k}+\mathbf{q},\mathbf{k}+\mathbf{q}',\mathbf{k}'+\mathbf{q}',\mathbf{k}'+\mathbf{q}}]$$
$$=-v^{k_y-k'_y}_{\mathbf{q}}(P^{eh}_{\mathbf{k}}-P^{eh}_{\mathbf{k}+\mathbf{q}})(P^{e'h'}_{\mathbf{k}'+\mathbf{q}}-P^{e'h'}_{\mathbf{k}'})+v^{q_y}_{\mathbf{k}-\mathbf{k}'}(P^{eh'}_{\mathbf{k}'+\mathbf{q}}-P^{eh'}_{\mathbf{k}+\mathbf{q}})(P^{e'h}_{\mathbf{k}}-P^{e'h}_{\mathbf{k}'})+O(E^6). \tag{13}$$

At low excitation intensities and for times small compared to the dephasing times, the coherent limit captures the essential physics of the nonlinear emission. In this case the pair-density correlation function, $N^{ehe'h'}_{\mathbf{k}_1,\mathbf{k}_2,\mathbf{k}_3,\mathbf{k}_4}$, vanishes and only the biexcitonic correlation function contributes. (Recently, Bartels *et al.* described experiments in which the pair density correlation function plays an important role.[63]) This function fulfills the fundamental anticommutation relations of Fermi particles, which are taken into account in an expansion of the form

$$B^{ehe'h'}_{\mathbf{k}+\mathbf{q},\mathbf{k},\mathbf{k}',\mathbf{k}'+\mathbf{q}}=\sum_{nm}\,[B^{ehe'h'}_{nm}(\mathbf{q})\varphi^{eh}_{n}(\mathbf{k}+\hat{\beta}\mathbf{q},q_y)\varphi^{e'h'}_{m}$$
$$\times(\mathbf{k}'+\hat{\alpha}\mathbf{q},-q_y)\pm B^{eh'e'h}_{nm}(\mathbf{k}-\mathbf{k}')\varphi^{eh'}_{n}$$
$$\times(\hat{\beta}\mathbf{k}+\hat{\alpha}\mathbf{k}'+\mathbf{q},k_y-k'_y)\varphi^{e'h}_{m}$$
$$\times(\hat{\beta}\mathbf{k}'+\hat{\alpha}\mathbf{k},k'_y-k_y)]\,, \tag{14}$$

where we assume the most general case of anisotropic masses in the y and z directions. In that case $\hat{\alpha}$ and $\hat{\beta}$ are diagonal matrices with $\alpha_{ii}=m_{ei}/M_i$, $\beta_{ii}=m_{hi}/M_i$, and $M_i=m_{ei}+m_{hi}$. Finally we take the physical limit $m_{ey}=m_{hy}\to\infty$. The expansion in terms of these eigenfunctions is performed in two steps. In the first step after insertion of Eq. (14) into Eq. (15), we multiply by the phase factor $\exp[il^2q_x(k_y-k'_y)]$ which appears in Eq. (14) from the Coulomb potential in the Landau gauge [Eq. (3)], and we perform the k_y and k'_y summations. This allows us to express the wave functions in Eq. (14) in the form,

$$\varphi^{eh}_{n}(k+\alpha q,p)=\sum_{k_y}\,\exp[il^2q_x(k_y+\alpha_{yy}q_y)]\varphi^{eh}_{n}(\mathbf{k}+\hat{\alpha}\mathbf{q},q_y), \tag{15}$$

which are solutions of the Wannier equation,

$$\frac{\hbar^2k^2}{2\mu^{eh}}\varphi^{eh}_{n}(k+\alpha q,p)-\sum_{k'}\,V^{(1)}(p,k-k')\varphi^{eh}_{n}(k'+\alpha q,p)$$
$$=\varepsilon^{eh}_{n}(pq)\varphi^{eh}_{n}(k+\alpha q,p), \tag{16}$$

with

$$V^{(1)}(p,k-k')=\frac{e^2}{2\pi\varepsilon_0 L}\int_0^\infty dp'p'$$
$$\times\frac{\exp[-(1/2)\,l^2p^2]}{p'^2+(k-k')^2}J_0(l^2pp'). \tag{17}$$

In the second step, we project Eq. (13) onto the basis set of these eigenstates; this results in the following equation of motion for the polarization,

$$\left(-i\hbar\frac{\partial}{\partial t}-\varepsilon^{eh}_{n}(0,0)\right)P^{eh}_{n}$$
$$=\boldsymbol{\mu}^{eh}\mathbf{E}\tilde{\varphi}^{eh}_{n}(0)-\sum_{ml}\sum_{e'h'}\,[(\boldsymbol{\mu}^{e'h}\mathbf{E}b^{eh'e'h'}_{nml}$$
$$+\boldsymbol{\mu}^{eh'}\mathbf{E}b^{e'he'h'}_{nml})P^{e'h}_{m}P^{e'h'*}_{l}]$$
$$+\sum_{mn'm'}\sum_{e'h'}V^{st}_{nm,n'm'}P^{e'h'*}_{m}P^{eh'}_{n'}P^{e'h}_{m'}$$
$$+\sum_{mn'm'}\sum_{e'h'}\sum_{\mathbf{q}}P^{e'h'*}_{m}[V^{c}_{nm,n'm'}(\mathbf{q})B^{ehe'h'}_{n'm'}(\mathbf{q})$$
$$\mp V^{xc}_{nm,n'm'}(\mathbf{q})B^{eh'e'h}_{n'm'}(\mathbf{q})], \tag{18}$$

where $\mathbf{q}$ now labels the two-dimensional vector $(q_\parallel,q_z)$. In Eq. (18), b_{nml} are the Pauli blocking matrix elements, V^{st} is the static Coulomb interaction, V^{c} is the random-phase-approximation Coulomb interaction, and V^{xc} is the corresponding exchange contribution. The definitions of the various matrix elements as well as those appearing Eq. (15) are summarized in the Appendix. The final form of the equation of motion of the biexcitonic correlation function is

$$\left(-i\hbar\frac{\partial}{\partial t}-\varepsilon^{eh}_{n}(\mathbf{q})-\varepsilon^{e'h'}_{m}(\mathbf{q})\right)B^{ehe'h'}_{nm}(\mathbf{q})$$
$$-\sum_{n'm'}\sum_{\mathbf{q}'}H_{nm,n'm'}(\mathbf{q},\mathbf{q}')B^{ehe'h'}_{n'm'}(\mathbf{q}')$$
$$=-\sum_{nm\mathbf{q}}\sum_{n'm'}(1-S)^{-1}_{nm\mathbf{q},\overline{nm\mathbf{q}}}\{V^{c}_{n'm',\overline{nm}}(\overline{\mathbf{q}})P^{eh}_{n'}P^{e'h'}_{m'}$$
$$-V^{xc}_{n'm',\overline{nm}}(\overline{\mathbf{q}})P^{eh'}_{n'}P^{eh'}_{m'}\}, \tag{19}$$

where H is the interaction matrix and S is the overlap integral. It is worth noting that the real-space representation of Eq. (19), written for infinite hole masses and with only the $1S$-exciton contributions retained, is nothing but the Heitler-London expansion.

Since the solution of Eqs. (18) and (19) is very time consuming, up to now only partial solutions of the problem have been performed. Most calculations have been performed in the second order Born approximation. The energies depend

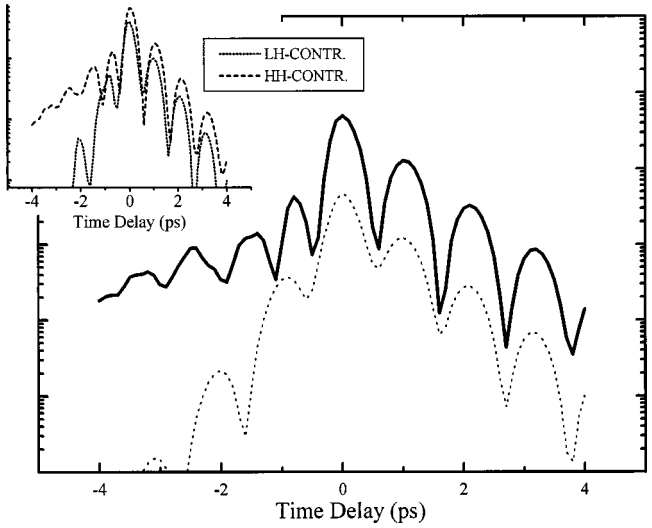

FIG. 13. TI-FWM for bulk GaAs in a high magnetic field calculated from the $\chi^{(3)}$ truncation scheme. The SBE result (dashed line) is shown for comparison. Inset: hh-X and lh-X contributions. The $\chi^{(3)}$ truncation scheme correctly yields the slow rise time of the TI-FWM and the quantum beats in the lh-X and hh-X signals.

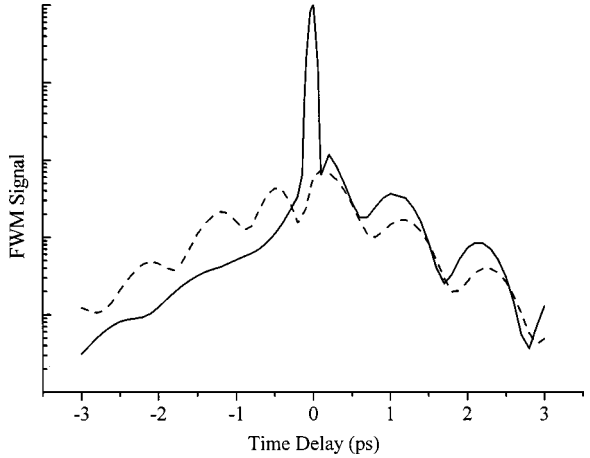

FIG. 14. TI-FWM for bulk GaAs in a high magnetic field calculated taking the $q_\parallel$ dependence of the biexcitonic correlation function into account (solid line). The calculation without the $q_\parallel$ dependence (dashed line) is shown for comparison. Including the $q_\parallel$ dependence smooths the oscillations for $\Delta t<0$ and reproduces the coherent peak.

only weakly on $q_\parallel$. Therefore, it is possible to simulate this dependency by a coarse grid, as long as the delay Δt is not too small. For Δt close to zero, interference effects in the continuum associated with $q_\parallel$ become important, and, even in the second-order Born approximation, it is not trivial to achieve convergence with respect to $q_\parallel$.

If contributions beyond this are taken into account, S_{TI}^{-} is expected to increase, since S_{TI}^{-} originates from the four-particle correlations. The interference of the different $q_\parallel$ contributions also damps out the structure for $\Delta t<0$. This means that the second-order Born approximation is well justified; it only underestimates the contribution for $\Delta t<0$.

Figure 13 shows the results of the calculation for the TI-FWM (solid curve). The results of the calculation without four-particle correlation effects—setting $B^{ehe'h'}_{k_1k_2k_3k_4}=0$—are also shown for comparison (dashed curve). The theory correctly reproduces the slow rise time seen experimentally in contrast to the calculation without four-particle correlations. The theoretical S_{TI}^{-}, however, has pronounced oscillations that are not seen in the experimental data.

These oscillations are smoothed out if the $q_\parallel$ dependency is taken into account more carefully, as shown in Fig. 14. This should be even more pronounced if contributions beyond the second-order Born approximation are accounted for. The coupling to the continuum associated with $q_\parallel$ correctly reproduces the coherent peak at $\Delta t=0$ seen in the experimental data.

The theory also agrees well with the experiment for the relative contributions of the lh-X and hh-X. This can be seen in the FWM-PS in Fig. 15 and in the inset to Fig. 13 which shows the area in the lh-X and hh-X peaks as a function of Δt. In contrast to the SBE calculation, the lh-X and hh-X contributions are of the same order of magnitude and the quantum beats are clearly seen at both frequencies. The exchange of oscillator strength between the lh-X and hh-X can also be seen in Fig. 15.

We have calculated the TI-FWM for a few different magnetic-field strengths B. As seen in Fig. 16, the increase of S_{TI}^{-} with B is well reproduced. For these calculations, the four-particle correlation rate $\gamma_B=0$ and the rise times are determined by the memory kernel of the correlation function.

The structure of the unbound biexcitons which is contained in the quantity $B^{ehe'h'}_{k_1k_2k_3k_4}$ clearly changes as the magnetic field is increased. The problem of the hydrogen molecule in strong magnetic fields, which is formally the same

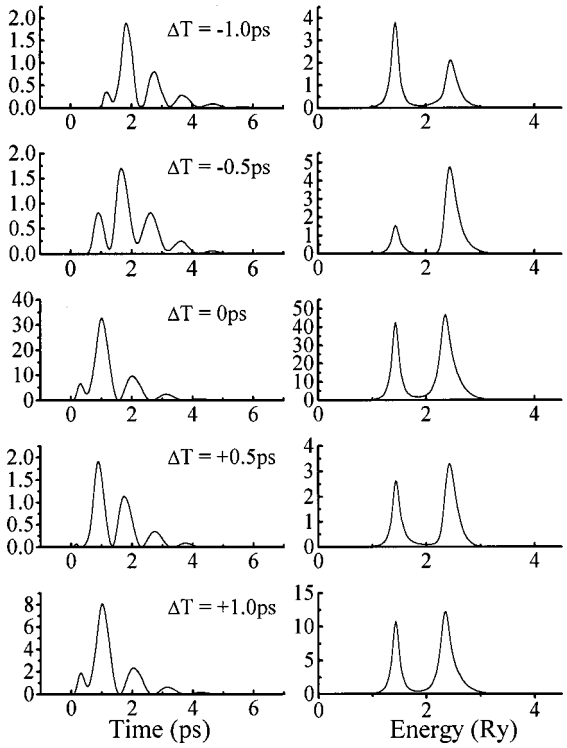

FIG. 15. TR-FWM and FWM-PS for different delays for bulk GaAs in a high magnetic field calculated from the $\chi^{(3)}$ truncation scheme, showing the quantum beats and exchange of oscillator strength induced by the four-particle correlations.

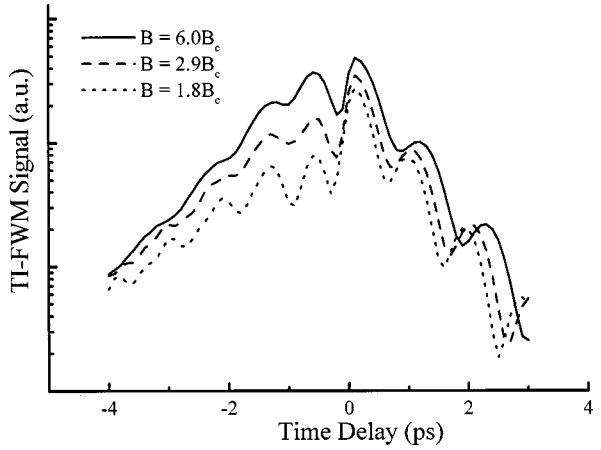

FIG. 16. TI-FWM for different magnetic-field strengths calculated from the $\chi^{(3)}$ truncation scheme, showing the increase in S_{TI}^{-} with magnetic field. All these curves are for high magnetic fields so the increase is not as dramatic as that seen in the experimental data.

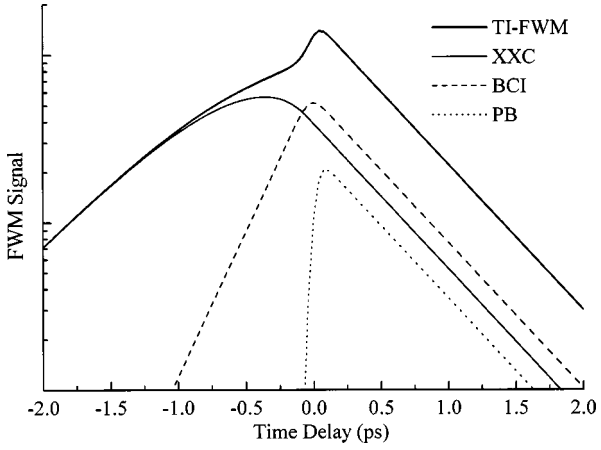

FIG. 17. Calculation of Eqs. (20) and (21). This model captures the essential physics of the full calculation and shows that S_{TI}^{-} is dominated by the signal due to four-particle correlations. For these curves, $P_s=1.12$, $\nu=0.05$, $a=10^{-4}$, $\gamma_P=0.001\ \mathrm{fs}^{-1}$, and $\gamma_B=0.001\ \mathrm{fs}^{-1}$.

as that of the biexciton, has been studied by many authors (see Refs. 28 and 29, and references therein). For the situation, $B\sim B_c$, which we are investigating, the magnetic energy and the Coulomb energy are of comparable strength and there is no straightforward perturbative solution for finding the energy states of the hydrogen molecule, but the problem has been solved for the case of a magnetic field parallel to the molecular axis using a numerical Hartree-Fock approach.[29] For the regime $0.18<B/B_c<\sim 14$, the ground state of the biexciton is the unbound state $^3\Sigma_u$ and the excitons can interact weakly via their quadrupole moments. It is possible that this quadrupole-quadrupole interaction is responsible for the strong four-particle correlations which become more pronounced as the quadrupole moment of the exciton grows with the magnetic field.

VI. AVERAGE POLARIZATION MODEL

Equations (18) and (19) can be reduced to a simple one-dimensional model by averaging over the lowest excitonic contributions.[21,52] The result is a set of equations in which there is only one polarization variable $P(t)$ and one four-particle correlation variable $B(t)$. The advantages of this simple model are that it captures the essential physics and yet is computationally much simpler. In fact it can be solved analytically in powers of the electric field for the case of δ-function excitation. In this ''average polarization model,'' the exciton-exciton scattering state continuum is modeled as a single resonance at twice the exciton frequency, i.e., at the edge of the biexciton continuum. We consider first the case of a single exciton. The equations are

$$\left[-i\frac{\partial}{\partial t}-i\gamma_P-\Omega_0\right]P(t)=-\mu\cdot\mathbf{E}+\mu\cdot\mathbf{E}\frac{|P(t)|^2}{P_s^2}+\nu P(t)|P(t)|^2+B(t)P(t)^* \tag{20}$$

and

$$\left[-i\frac{\partial}{\partial t}-i\gamma_B-2\Omega_0\right]B(t)=aP(t)^2. \tag{21}$$

Equation (20) has the structure of a single resonance driven by four terms. The first term is simply the driving electric field and is responsible for the linear response of the polarization. The second term, $\propto E|P(t)|^2$, is the effect of Pauli blocking (PB), or phase-space filling, on the excitation. The third term comes from the Coulomb interaction between the excitons in the Hartree-Fock approximation. This term, referred to as the bare Coulomb interaction (BCI) term, is responsible for the $\Delta t<0$ signal which, as mentioned before, has a rise time of $1/4\gamma$.

The last term in Eq. (20) is the contribution of four-particle correlations to the polarization. Here B is the effective four-particle correlation whose equation of motion is Eq. (21). The parameter a is the strength of the exciton-exciton correlation (XXC), i.e., the coupling of B to P. Figure 17 shows the results of a calculation of the model with the parameters P_s, ν, and a chosen to reproduce the line shape of the experimental curves (absent the quantum beats, of course). The three other curves are the contributions to the total signal from PB, BCI, and XXC. The nonexponential curvature at small $\Delta t<0$, and the very long rise time of S_{TI}^{-} are easily understood by formally integrating Eq. (21) to express the XXC source term of Eq. (20),

$$B(t)P(t)^*\propto\ a\,P(t)^*\int_{-\infty}^{t}dt'\,P(t')^2e^{(i2\Omega_0-\gamma_B)(t-t')}.$$

This term is obviously of the same order as the PB and BCI contributions. However, it has a completely different time dependence. It grows first as the integral of the square of the polarization before exhibiting an exponential decay determined by γ_B, the dephasing rate of B. It is the dominant source of the FWM signal for $\Delta t<0$, and characterizes a coherent memory stored in the four-particle correlations. Thus B can be viewed as a non-Markovian source for the polarization. It is interesting to note that all three contributions decay at the rate $2\gamma_P$ for S_{TI}^{+}. Therefore, although one

cannot distinguish between PB, BCI, and XXC in S_{TI}^{+}, the decay of S_{TI}^{+} unambiguously yields γ_P. By construction, Eqs. (20) and (21) only account for a single resonance, and thus do not include quantum beats. However, they reproduce the trends of the experimental observations.

Extending the model to include both the lh-X and hh-X for σ^- excitation is straightforward.

$$\left[-i\frac{\partial}{\partial t}-i\gamma_P-\Omega_{hh}\right]P^a(t) = -\mu_{\mathbf{hh}}\cdot\mathbf{E}\left(1-\frac{|P^a(t)|^2}{P_s^2}\right)+\nu P^a(t)|P^a(t)|^2 + P^a(t)*B^{aa}(t)+P^b(t)*B^{ab}(t), \tag{22}$$

$$\left[-i\frac{\partial}{\partial t}-i\gamma_P-\Omega_{lh}\right]P^b(t) = -\mu_{\mathbf{lh}}\cdot\mathbf{E}\left(1-\frac{|P^b(t)|^2}{P_s^2}\right)+\nu P^b(t)|P^b(t)|^2 + P^b(t)*B^{bb}(t)+P^a(t)*B^{ab}(t), \tag{23}$$

and

$$\left[-i\frac{\partial}{\partial t}-i\gamma_B-2\Omega_{hh}\right]B^{aa}(t)=V_{aa}P^a(t)^2, \tag{24}$$

$$\left[-i\frac{\partial}{\partial t}-i\gamma_B-2\Omega_{lh}\right]B^{bb}(t)=V_{bb}P^b(t)^2, \tag{25}$$

$$\left[-i\frac{\partial}{\partial t}-i\gamma_B-\Omega_{hh}-\Omega_{lh}\right]B^{ab}(t)=V_{ab}P^a(t)P^b(t). \tag{26}$$

The superscript a refers to the hh transition from the $m_J=+3/2$ valence band to the $m_s=+1/2$ conduction band, and the superscript b refers to the lh transition from the $m_J=+1/2$ valence band to the $m_s=-1/2$ conduction band. B^{ab} refers to the four-particle correlation between the lh-X and hh-X.

Figure 18 gives some of the TI-FWM results showing that the quantum beats are due solely to the four-particle correlations and that the strength of the lh-X signal is increased by the four-particle correlations. Figure 18(a) shows the lh-X and hh-X contributions to the signal in which the increase in the lh-X signal due to B^{ab} is evident. In Fig. 18(b) the different contributions to the TI-FWM from the different nonlinearities are plotted. Only the XXC signal shows strong oscillations, but very weak oscillations due to polarization interference are seen in the PB contribution. Figure 19 gives some of the TR-FWM results. Figure 19(a) shows the contributions of the different nonlinearities to the TR-FWM signal. Note that each nonlinearity has a different rise time. Figure 19(b) shows the TR-FWM signals at different delays. In all these calculations the values of the various parameters have been adjusted to reproduce the overall experimental results whereas the curves of Figs. 13, 14, 15, and 16 are obtained from first principles. Nevertheless the model is almost trivial to solve numerically, and gives a direct insight into the PB, BCI, and XXC contributions to the FWM.

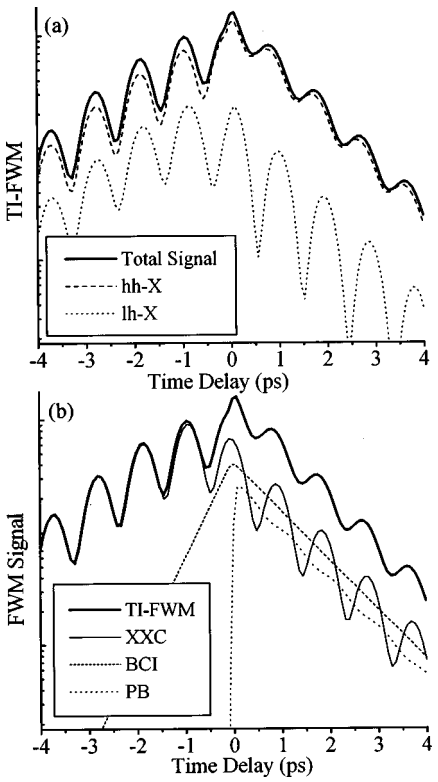

FIG. 18. TI-FWM calculated from Eqs. (22)–(26) for the parameter values $P_s=1$, $\nu=10^{-3}$, $V_{aa}=V_{bb}=V_{ab}=10^{-6}$, $\gamma_P=0.0005\,\mathrm{fs}^{-1}$, and $\gamma_B=0.0005\,\mathrm{fs}^{-1}$. In (a) the dotted line is the lh-X contribution and the dashed line is the hh-X contribution. The solid line is the total signal. In (b) the dotted line is the PB contribution, the dashed line is the BCI contribution, and the thin solid line is the XXC contribution. The heavy solid line is the total signal. Here we see that the quantum beating is due entirely to XXC.

VII. PROPERTIES OF THE FOUR-PARTICLE CORRELATIONS

Although n-particle correlations play an important role in many-body theory, experimentally these objects are rarely accessed directly. Most of the time they are inferred from the changes brought about in a linear response by external constraints. The magnetic-field enhancement of the four-particle correlations and the possibility of selecting the time delay where their contribution to the FWM is dominant provide us with a rare opportunity to study these objects directly. Here we are dealing with unbound four-particle correlations which are not revealed by a resonance in the spectrum as are bound biexcitons, and whose decoherence has never been investigated before, to our knowledge. In this section we discuss three experiments done at high magnetic field ($B=10$ T) where there is a strong signal due to four-particle correlations and where, by changing other parameters of the system, we can study their nature and properties.

By changing the exciton density, the length scales over which four-particle correlations persist can be studied as can their sensitivity to density. Figure 20 shows a series of TI-FWM curves for different densities between $N\approx10^{17}$ and

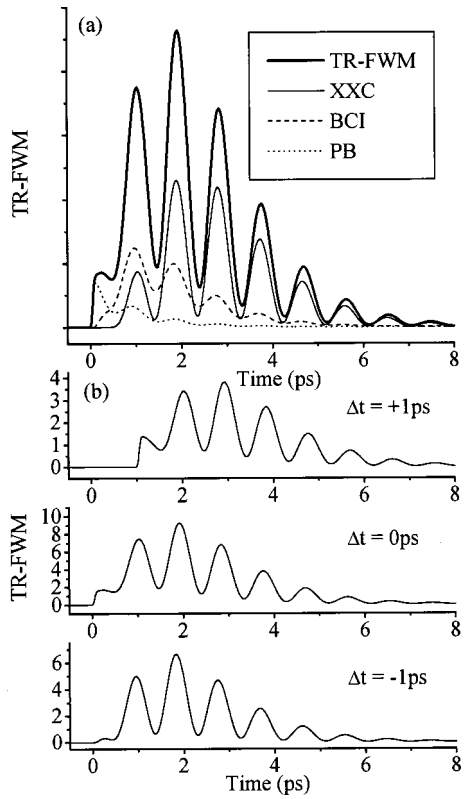

FIG. 19. TR-FWM calculated from Eqs. (22)–(26) for the same parameters as in Fig. 18. In (a) the dotted line is the PB contribution, the dashed line is the BCI contribution, and the thin solid line is the XXC contribution. The heavy solid line is the total signal. (b) TR-FWM for various time delays. The curves in (a) show that the different contributions to the signal (PB, BCI and XXC) have different rise times.

$N \approx 5 \times 10^{14}\,\mathrm{cm}^{-3}$. We change the density by changing the laser intensity, so, in all cases, we are dealing with an initially coherent population. At the lowest density (the lowest curve in Fig. 20), $S_{TI}^{-} > S_{TI}^{+}$ and has the slow rise time, both of which indicate the presence of four-particle correlations. At this density the average separation between excitons is $\sim 9a_0$, where a_0 is the zero-field exciton Bohr radius. Because the correlations are in scattering states (not bound biexcitons), it is reasonable to assume that the exciton distribution is uniform and the excitons are correlated over distances of $\approx 9a_0$. It is remarkable that the four-particle correlations exist over such large distances.

At high densities, S_{TI}^{-} has a shape consistent with the mean-field theory. $S_{TI}^{-} < S_{TI}^{+}$ and $\tau_r = \tau_d/2$. In fact, it is interesting to note that the data at high density and high magnetic field are in better agreement with the mean-field theory than the data at $B = 0$ T and low density. At high densities, the excitons are close together, so that each exciton is able to interact with many of its neighbors over the time scale of the experiment. This is exactly the regime in which mean-field theory is valid. As the density is increased, we also expect the screening to increase, but (i) here we are dealing mainly with an exciton gas for which screening is weaker and can be treated as wavevector independent;[64] and (ii) the nearest neighbor distance $r \propto N^{-1/3}$ decreases faster than the interaction length which, even for Thomas-Fermi screening, is

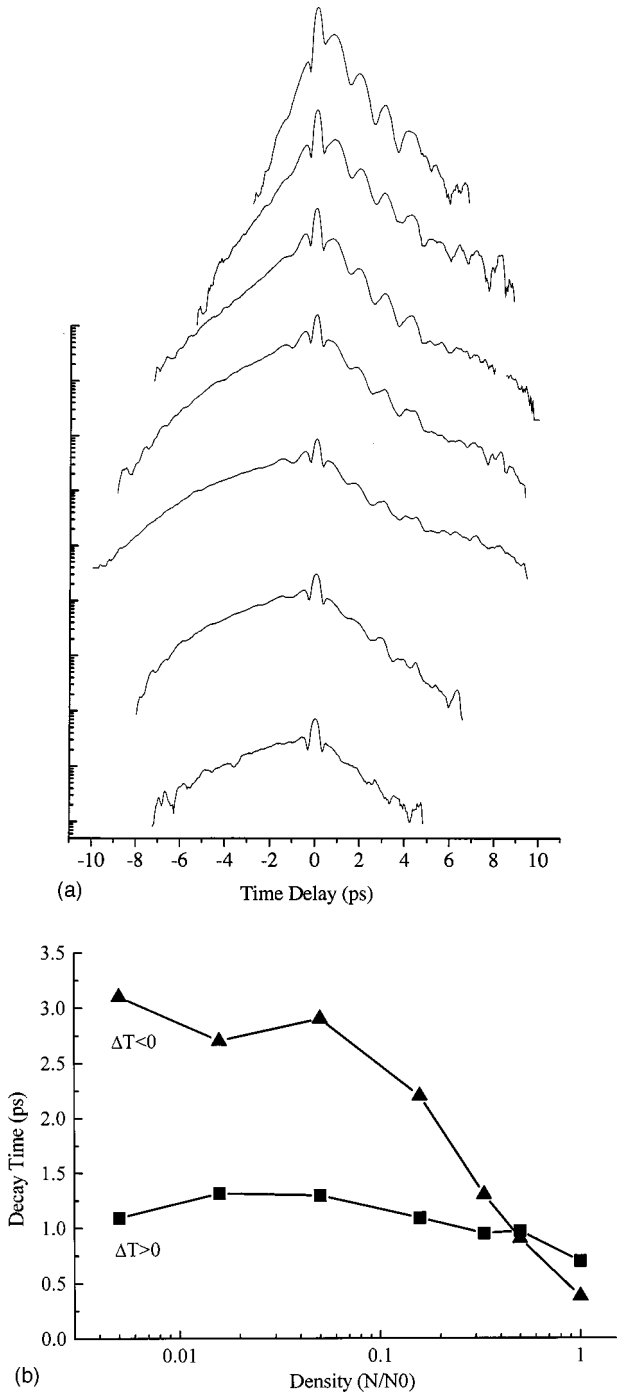

FIG. 20. (a) TI-FWM for different densities at $B = 10$ T. The curves are plotted on a logarithmic scale and displaced for clarity. From top to bottom the densities are $N \approx 10^{17}\,\mathrm{cm}^{-3}$, $N/2$, $N/3$, $N/6$, $N/20$, $N/63$, and $N/200$. (b) τ_r (triangles) and τ_d (squares) vs N. $N0 \approx 10^{17}\,\mathrm{cm}^{-3}$. At high density the curves are in agreement with the SBE, but at low densities the XXC signal dominates for $\Delta t < 0$.

$\lambda_{TF} \propto N^{-1/6}$. Therefore, what is observed is indeed the establishment of the mean-field regime. We see that the transition occurs at an average exciton-exciton separation of $\sim 2a_0$. Below this density, the mean free time for exciton-exciton scattering is of the order of the rise time of the FWM signal. Not enough scattering events occur over the time span of the experiment for the mean-field conditions to be established.

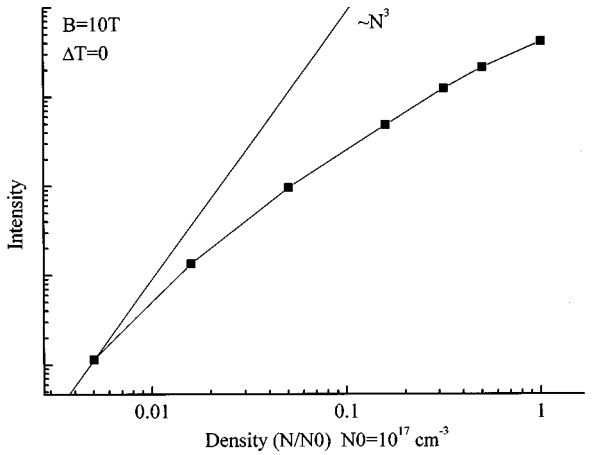

FIG. 21. Intensity of the FWM at $\Delta t=0$ vs input laser intensity, showing that, at these densities, we are not in the $\chi^{(3)}$ regime.

Thus what is observed in that case are the deviations from the mean-field theory, i.e., the fluctuations in exciton-exciton scattering which are accounted for by $B^{ehe'h'}_{k_1k_2k_3k_4}$.

As is clear from Fig. 20, we are not in the $\chi^{(3)}$ regime where $S_{TI}(\Delta t=0)\propto I^3$. This is shown more clearly in Fig. 21, where $S_{TI}(\Delta t=0)$ is plotted against the input intensity. This is in agreement with recent work[65] that showed that in bulk GaAs (at zero magnetic field) at densities as low as 2×10^{14} cm^{-3} the FWM signal is still not in the $\chi^{(3)}$ regime. Many-body effects which cannot be well described by an expansion in powers of the electric field play an important role even at densities where the excitons are very far apart.

Another important question about four-particle correlations is their coherence. In almost all experiments performed thus far, only the coherence of the excited electron-hole pairs have been measured, but there is coherence associated with the higher-order correlations as well. From the TI-FWM we can obtain information about the coherence of both the exciton and the four-particle correlations. As we have seen in previous sections, the exciton dephasing time can always be determined from the decay of S^+_{TI}, and the four-particle coherence influences S^-_{TI}. Determining the four-particle dephasing time is not as simple because the rise time of S^-_{TI} is a function of both the exciton dephasing time and the four-particle dephasing time as well as the strengths of the BCI and XXC nonlinearities. Nevertheless, we can still extract information about the coherence of the four-particle correlations from the behavior of S^-_{TI}.

One test of the coherence of the four-particle correlations is carrier density. By changing the detuning of the laser, we can change the relative excitation density of bound excitons and free e-h pairs as well as the total excitation density excited by the laser. In this way we can study how both free carriers and bound excitons affect the four- and two-particle coherences. In this case we are always studying initially coherent populations. The effect of incoherent populations on the two-particle coherence has been investigated by Schultheis *et al.*[66,67] Three curves are shown in Fig. 22. The middle curve is for approximately zero detuning, i.e., the center frequency of the laser tuned between the lh-X and hh-X. The top curve is for negative detuning, laser tuned to lower energy, and the bottom curve is for positive detuning.

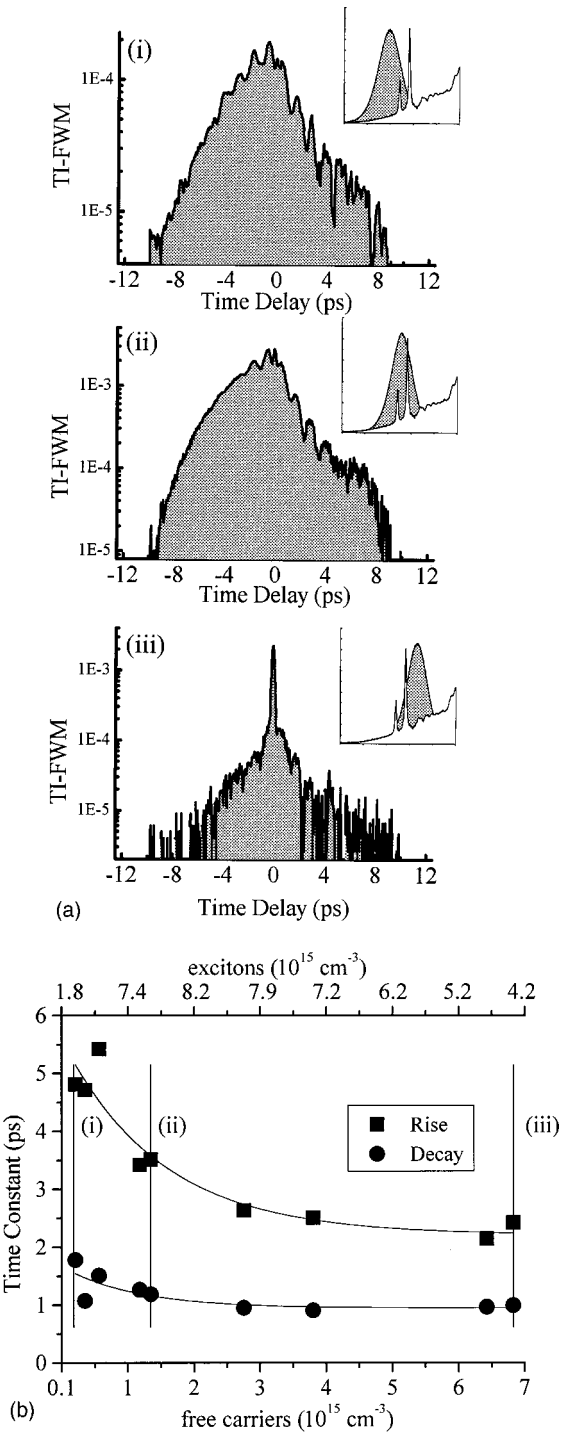

FIG. 22. (a) TI-FWM for (i) negative, (ii) zero and (iii) positive detunings of the laser pulse. $B=10$T insets: laser spectrum and absorption spectrum. (b) τ_r and τ_d vs free-carrier density. Vertical lines correspond to the three measurements shown in (a). The top axis gives the exciton density. Solid lines are guides for the eye. In these curves, we see a decrease in the rise and decay times with increasing free carrier density.

At zero detuning the signal is pretty much the same as in the previous figures. S^-_{TI} is large and has only about one oscillation near $\Delta t=0$. At negative detuning S^-_{TI} becomes significantly larger in comparison with S^+_{TI}. Also, there are large oscillations in S^-_{TI}. As we discuss in Sec. V, the lack of oscillations in S^-_{TI} for zero detuning is due largely to exciton-

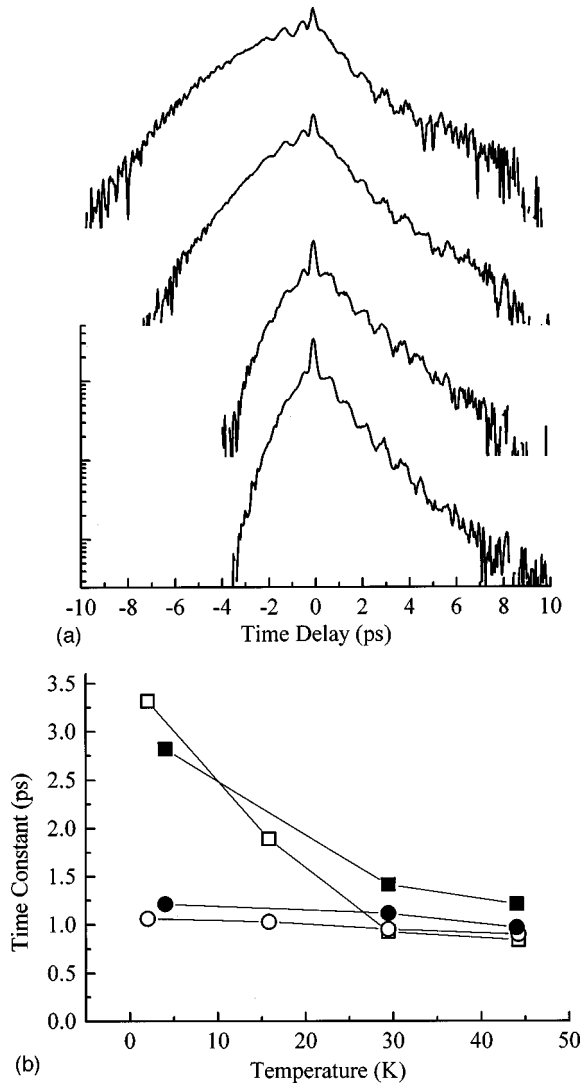

FIG. 23. (a) TI-FWM for temperatures 2, 16, 29, and 44 K (from top to bottom) for sample No. 1. (b) τ_r (squares) and τ_d (circles) vs T. Solid symbols are for sample No. 2. As the temperature is increased, τ_r decreases, but τ_d remains roughly the same, indicating that the coherence of four-particle correlations is destroyed more rapidly with temperature.

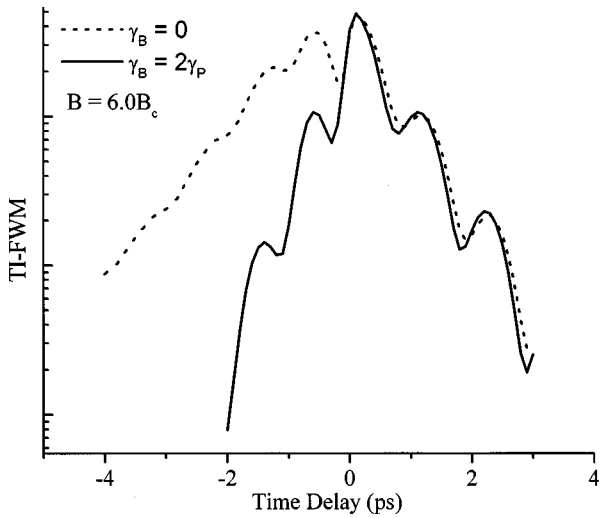

FIG. 24. Calculation of TI-FWM in the $\chi^{(3)}$-truncation scheme: the solid line is for $\gamma_B = 2\gamma_P$ and the dashed line is for $\gamma_B = 0$. Increasing the dephasing rate of the four-particle correlations destroys S_{TI}^{-} in the same manner as increasing the temperature.

exciton correlations with $q_{\|} \neq 0$. At negative detuning, the coupling to the continuum associated with $q_{\|} \neq 0$ becomes less important, and the oscillations in S_{TI}^{-} become more pronounced. It is also remarkable that the maximum of S_{TI}^{-} is larger than the coherent peak at $\Delta t = 0$. At positive detuning the coherent peak dominates the signal and the magnitude and rise time of S_{TI}^{-} are much diminished, although the rise time is not $T_2/2$, indicating that we are not in the mean-field regime.

Here we are clearly seeing the effects of free carriers on the four-particle coherence. For the negative detuning [Fig. 22(a), part (i)], there are only, $N_{eh} \approx 2 \times 10^{14}$ cm^{-3} free carriers excited, whereas for the case of positive detuning there are $N_{eh} \approx 7 \times 10^{15}$ cm^{-3} free carriers excited. In Fig. 22(b) we plot the rise and decay times verse the free carrier density. The vertical lines show the three measurements from Fig. 22(a). On the top axis, the corresponding exciton density is shown. Note that the exciton density is not linear with respect to the x axis and that it changes by less than a factor of 5 while the free-carrier density changes by more than a factor of 50. Clearly the rise and decay times are more strongly dependent on the free-carrier density than on the exciton density. The detuning experiment is difficult to interpret because the detuning affects the strength of the nonlinearities in addition to affecting the dephasing parameters. In the ''average polarization'' model it is, however, possible to reproduce the overall shape of Fig. 22 with the signal maximum at $\Delta t < 0$ by adjusting the strength of the XXC nonlinearity and the four-particle dephasing time.

Studying the effect of temperature on the dephasing should be easier to interpret because the only parameters affected by temperature are the dephasing parameters which account for all phonon interactions. Figure 23 shows a series of TI-FWM curves for four different temperatures between 2 and 44 K. The magnetic field was kept at $B = 10$ T. The laser was again tuned between the lh-X and hh-X. As the temperature is increased, the band edge shifts to lower energy and the laser is retuned to keep the overlap with the exciton peaks roughly the same. The density of excited e-h pairs is roughly $N \approx 10^{16}$ cm^{-3}, corresponding to an average distance between pairs of 40 nm$\approx 3.3a_0$. Between 2 and 44 K, τ_d changes only slightly. In contrast τ_r changes by more than a factor of 3. We estimate τ_r from the slope of S_{TI}^{-} between $\Delta t = -2$ and -0.5 ps, and τ_d from the slope of S_{TI}^{+} between $\Delta t = 0.5$ and 2 ps. The rise and decay times are shown plotted against temperature in the inset to Fig. 23. The large change in S_{TI}^{-} compared with S_{TI}^{+} shows that the four-particle correlation is more strongly affected by temperature than the two-particle correlation.

The theory does not include explicitly phonon interactions, so that all temperature effects are included in the dephasing parameters, γ_P and γ_B. Thus, to model the effects of temperature shown in Fig. 23, we have made a calculation of the full theory with $\gamma_B = 2\gamma_P$. In fact, because of off-diagonal contributions to the microscopic decoherence of

$B^{ehe'h'}_{k_1k_2k_3k_4}$, it is always the case that $\gamma_B \leqslant 2\gamma_P$. The resulting TI-FWM is shown in Fig. 24. For comparison, the curve with $\gamma_B = 0$ is also shown. We see that increasing γ_B reduces S^-_{TI} in the same manner as increasing the temperature does experimentally. We have also calculated the effects of both LO and acoustic phonons on the four-particle correlation dephasing from the microscopic theory. We found that the calculated effect of phonons on the dephasing is two orders of magnitude too small to account for the observed change, although the phonons affect the four-particle correlation dephasing more than that of excitons. We have also considered the possibility that increased continuum absorption is responsible for the dephasing due to a temperature-dependent shift in the continuum edge, but this is also not the case. At present the temperature effect remains unexplained.

VIII. CONCLUSION

We have studied exciton-exciton correlations (four-particle correlations) in bulk GaAs in magnetic fields from 0 T, where no correlations are seen, to 10 T where strong correlations are seen. To our knowledge, this is the first time that exciton-exciton correlations in the scattering state continuum have been studied. We have shown that the magnetic field strongly enhances these correlations, and have studied the exciton-exciton correlations under a variety of conditions, demonstrating the long range of the correlations and the sensitivity of the exciton-exciton coherence as compared to the exciton coherence.

Furthermore, the exciton-exciton correlations represent deviations from the mean-field regime and, as such, are of inherent interest in condensed-matter physics where mean-field theories have been a powerful tool for explaining many phenomena. This work shows the power of nonlinear spectroscopy for investigating many-body physics beyond mean-field theory and other questions of interest that are inaccessible to linear-response theory.

ACKNOWLEDGMENTS

We have the pleasure to acknowledge very fruitful discussions with Professor L. J. Sham, Professor D.-H. Lee, and Dr. S. Dodge. We would like to thank both Sandia National Laboratories and Bell Labs for providing us with high-quality GaAs samples. This work was supported by the Director, Office of Energy Research, Office of Basic Energy Sciences, Division of Material Sciences of the U.S. Department of Energy, under Contract No. DE-AC03-76SF00098.

APPENDIX: MATRIX ELEMENTS

For better readability we represent $\mathbf{q}$ as (p,q). The Pauli blocking matrix element is given by

$$b^{eh'e'h'}_{nml} = \sum_k \varphi^{eh}_n(k,0)\varphi^{eh'}_m(k,0)\varphi^{e'h'}_l(k,0). \tag{A1}$$

The static Coulomb interaction in the equation of motion for the polarization reads as

$$V^{st}_{nm,n'm'} = \sum_{k,q} V^{(1)}(0,k-q)\varphi^{eh'}_{n'}(k)\,\varphi^{e'h}_{m'}(q,0)[\varphi^{eh}_n{}^*(k,0) - \varphi^{eh}_n{}^*(q,0)][\varphi^{e'h'}_m{}^*(q,0) - \varphi^{e'h'}_m{}^*(k,0)]. \tag{A2}$$

The two other Coulomb matrix elements in the mentioned equation, the random-phase-approximation-like V^c and exchange-type V^{xc} are defined as

$$V^c_{nm,n'm'}(q,p) = v^0(q,p)M^{eh}_{nn'}(q,p)M^{e'h'}_{mm'}(q,p) \tag{A3}$$

$$V^{xc}_{nm,n'm'}(q,p) = \sum_{kk'} v^0(q,p)\varphi^{eh}_n{}^*(k+\alpha q,0)\varphi^{e'h'}_m{}^*(k+\beta q,0)[\varphi^{eh'}_{n'}(k,p) - \varphi^{eh'}_{n'}(k',p)][\varphi^{eh'}_{m'}(k'+q,p) - \varphi^{eh'}_{m'}(k+q,p)], \tag{A4}$$

where we made use of the Coulomb interaction

$$v^{p'}(q,p) = \frac{e^2}{2\pi\varepsilon_0 L^2} p \frac{\exp[(1/2)\,l^2p^2]}{p^2+q^2} J_0(l^2pp'), \tag{A5}$$

and the overlap matrix elements

$$M^{eh}_{nn'}(q,p) = \sum_k \varphi^{eh}_n{}^*(k,0)[\varphi^{eh}_{n'}(k+\alpha q,p) - \varphi^{eh}_{n'}(k-\beta q,p)]. \tag{A6}$$

The overlap matrix is defined by

$$S_{nm\mathbf{q},n'm'\mathbf{q}'}=\sum_k \varphi_n^{eh*}(k+q'+\beta q,p)\varphi_m^{e'h'*}(k+\alpha q,p)\varphi_{n'}^{eh'}(k+q+\beta q',p')\varphi_{m'}^{e'h}(k+\alpha q',p')J_0(l^2pp'). \tag{A7}$$

The interaction matrix H in Eq. (19) is obtained by applying $(1-S)^{-1}$ to a matrix $\tilde{H}$:

$$H_{nm,n'm'}(\mathbf{q},\mathbf{q}')=\sum_{\overline{nm}}\sum_{\overline{\mathbf{q}}}(1-S)^{-1}_{nm,\overline{nm}}(\mathbf{q},\overline{\mathbf{q}})\tilde{H}_{\overline{nm},n'm'}(\overline{\mathbf{q}},\mathbf{q}'). \tag{A8}$$

This is finally given by

$$\begin{aligned}\tilde{H}_{nm,n'm'}(\mathbf{q},\mathbf{q}')=&V^{(2)}(q-q',p,p')\{\overline{M}^{eh}_{nn'}(\beta(q-q'),p,p')\overline{M}^{eh}_{mm'}(\alpha(q-q'),p,p')+\overline{M}^{eh}_{nn'}(\alpha(q-q'),p,p')\\&\times\overline{M}^{eh}_{mm'}(\beta(q-q'),p,p')\}-V^{(3)}(q-q',p,p')\{\overline{M}^{eh}_{nn'}(\beta(q-q'),p,p')\overline{M}^{eh}_{mm'}(\beta(q'-q),p,p')\\&+\overline{M}^{eh}_{nn'}(\alpha(q'-q),p,p')\overline{M}^{eh}_{mm'}(\alpha(q-q'),p,p')\}\pm\sum_{kk'}\varphi_n^{eh*}(k+\beta(q-q'),p)\varphi_m^{e'h'*}(k'+\alpha(q+q'),p)\\&\times[V^{(1)}(p,q'-k')J_0(l^2pp')\{\varphi_{n'}^{eh'}(k',p')\,\varphi_{m'}^{e'h}(k'+\beta(q-q')+\alpha(q+q'),p')+\varphi_{n'}^{eh'}(k,p')\\&\times\varphi_{m'}^{e'h}(k+\beta(q-q')+\alpha(q+q'),p')\}-V^{(4)}(q-q',p,p')\{\varphi_{n'}^{eh'}(k',p')\\&\times\varphi_{m'}^{e'h}(k'+\beta(q-q')+\alpha(q+q'),p')+\varphi_{n'}^{eh'}(k,p')\varphi_{m'}^{e'h}(k+\beta(q-q')+\alpha(q+q'),p')\}],\end{aligned} \tag{A9}$$

where $\overline{M}$ is given by

$$\overline{M}^{eh}_{nn'}(q,p,p')=\sum_k \varphi_n^{eh}(k,p)\varphi_{n'}^{eh}(k+q,p'), \tag{A10}$$

and the various Coulomb matrices are defined according to

$$V^{(2)}(q-q',p,p')=\frac{e^2}{2\pi\varepsilon_0 L}\int_0^{2\pi}\frac{d\phi}{2\pi}\frac{\exp[(1/2)\,l^2(p^2+p'^2-2pp'\cos\,\phi)]}{p^2+p'^2-2pp'\cos\phi+(q-q')^2}, \tag{A11}$$

$$V^{(3)}(q-q',p,p')=\frac{e^2}{2\pi\varepsilon_0 L}\int_0^{2\pi}\frac{d\phi}{2\pi}\frac{\exp[(1/2)\,l^2(p^2+p'^2-2pp'\cos\phi)]}{p^2+p'^2-2pp'\cos\phi+(q-q')^2}\cos(l^2pp'\sin\phi), \tag{A12}$$

$$V^{(4)}(q-q',p,p')=\frac{L^2}{2\pi}\int_0^{\infty}dp''p''V^{(3)}(q-q',p,p'')J_0(l^2p''p') \tag{A13}$$

---

*Present address: School of Physics and Astronomy, Tel Aviv University, Ramat-Aviv 69978, Tel Aviv, Israel.

†Present address: Instituto de Física, Universidade Estadual de Campinas, Caixa Postal 6165, 13083-970 Campinas-SP, Brazil.

‡Former name: Höchstleistungsrechenzentrum.

[1] S. Schmitt-Rink and D. S. Chemla, Phys. Rev. Lett. **57**, 2752 (1986).

[2] K. Leo, M. Wegener, J. Shah, D. S. Chemla, E. O. Göbel, T. C. Damen, S. Schmitt-Rink, and W. Schäfer, Phys. Rev. Lett. **65**, 1340 (1990).

[3] D. S. Chemla, J.-Y. Bigot, M.-A. Mycek, and S. Weiss, Phys. Rev. B **50**, 8439 (1994).

[4] D.-S. Kim, J. Shah, T. C. Damen, W. Schäfer, F. Jahnke, S. Schmitt-Rink, and K. Koöhler, Phys. Rev. Lett. **69**, 2725 (1992).

[5] S. Bar-Ad, I. Bar-Joseph, G. Finkelstein, and Y. Levinson, Phys. Rev. B **50**, 18 375 (1994).

[6] E. J. Mayer, G. O. Smith, V. Heuckeroth, J. Kuhl, K. Bott, A. Schulze, T. Meier, S. W. Koch, P. Thomas, R. Hey, and K. Ploog, Phys. Rev. B **51**, 10 909 (1995).

[7] H. Nickolaus and F. Henneberger, Phys. Rev. B **57**, 8774 (1998).

[8] D. Bennhardt, P. Thomas, R. Eccleston, E. J. Mayer, and J. Kuhl, Phys. Rev. B **47**, 13 485 (1993).

[9] T. Rappen, U. Peter, and M. Wegener, Phys. Rev. B **49**, 10 774 (1994).

[10] V. M. Axt, A. Stahl, E. J. Mayer, P. H. Bolivar, S. Nüsse, K. Ploog, and K. Köhler, Phys. Status Solidi B **188**, 447 (1995).

[11] H. Wang, K. Ferrio, and D. G. Steel, Phys. Rev. Lett. **71**, 1261 (1993).

[12] G. Bartels, G. C. Cho, T. Dekorsy, H. Kurz, and A. Stahl, Phys. Rev. B **55**, 16 404 (1997).

[13] F. C. Spano and S. Mukamel, Phys. Rev. A **40**, 5783 (1989).

[14] F. C. Spano and S. Mukamel, Phys. Rev. Lett. **66**, 1197 (1991).

[15] S. Mukamel, *Principles of Nonlinear Optical Spectroscopy* (Oxford University Press, New York, 1995).

[16] K. Victor, V. M. Axt, and A. Stahl, Phys. Rev. B **51**, 14 164 (1995).

[17] M. Z. Maialle and L. J. Sham, Phys. Rev. Lett. **73**, 3310 (1994).

[18] R. Binder and S. W. Koch, Prog. Quantum Electron. **19**, 307 (1995).

[19] I. E. Perakis, Chem. Phys. **210**, 259 (1996).
[20] P. Kner, S. Bar-Ad, M. V. Marquezini, D. S. Chemla, and W. Schäfer, Phys. Rev. Lett. **78**, 1319 (1997).
[21] P. Kner, S. Bar-Ad, M. V. Marquezini, D. S. Chemla, and W. Schäfer, Phys. Status Solidi A **164**, 579 (1997).
[22] P. Kner, W. Schäfer, R. Lövenich, and D. S. Chemla, Phys. Rev. Lett. **81**, 5386 (1998).
[23] S. Glutsch, U. Siegner, M.-A. Mycek, and D. S. Chemla, Phys. Rev. B **50**, 17 009 (1994).
[24] U. Siegner, M.-A. Mycek, S. Glutsch, and D. S. Chemla, Phys. Rev. Lett. **74**, 470 (1995).
[25] U. Siegner, M.-A. Mycek, S. Glutsch, and D. S. Chemla, Phys. Rev. B **51**, 4953 (1995).
[26] S. Bar-Ad, P. Kner, M. V. Marquezini, S. Mukamel, and D. S. Chemla, Phys. Rev. Lett. **78**, 1363 (1997).
[27] R. J. Elliott and R. Loudon, J. Phys. Chem. Solids **15**, 196 (1960).
[28] Y. P. Kravchenko, M. A. Liberman, and B. Johansson, Phys. Rev. A **54**, 287 (1996).
[29] Y. P. Kravchenko and M. A. Liberman, Phys. Rev. A **57**, 3403 (1998).
[30] C. Stafford, S. Schmitt-Rink, and W. Schaefer, Phys. Rev. B **41**, 10 000 (1990).
[31] M. Jiang, H. Wang, R. Merlin, D. G. Steel, and M. Cardona, Phys. Rev. B **48**, 15 476 (1993).
[32] T. Rappen, G. Mohs, and M. Wegener, Appl. Phys. Lett. **63**, 1222 (1993).
[33] O. Carmel and I. Bar-Joseph, Phys. Rev. B **47**, 7606 (1993).
[34] S. T. Cundiff, M. Koch, W. H. Knox, and J. Shah, Phys. Rev. Lett. **77**, 1107 (1996).
[35] J. B. Stark, W. H. Knox, and D. S. Chemla, Phys. Rev. Lett. **65**, 3033 (1990).
[36] T. Yajima and Y. Taira, J. Phys. Soc. Jpn. **47**, 1620 (1979).
[37] H. Haug and S. W. Koch, *Quantum Theory of the Optical and Electronic Properties of Semiconductors* (World Scientific, Singapore, 1993).
[38] S. Schmitt-Rink, D. S. Chemla, and H. Haug, Phys. Rev. B **37**, 941 (1988).
[39] S. Weiss, M.-A. Mycek, J.-Y. Bigot, S. Schmitt-Rink, and D. S. Chemla, Phys. Rev. Lett. **69**, 2685 (1992).
[40] M. Wegener, D. S. Chemla, S. Schmitt-Rink, and W. Schäfer, Phys. Rev. A **42**, 5675 (1990).
[41] M. Lindberg, R. Binder, and S. W. Koch, Phys. Rev. A **45**, 1865 (1992).
[42] S. Glutsch, U. Siegner, and D. S. Chemla, Phys. Rev. B **52**, 4941 (1995).
[43] M. Lindberg and S. W. Koch, Phys. Rev. B **38**, 3342 (1988).
[44] F. Jahnke, M. Koch, T. Meier, J. Feldmann, W. Schäfer, P. Thomas, S. W. Koch, E. O. Göbel, and H. Nickel, Phys. Rev. B **50**, 8114 (1994).
[45] Y. Z. Hu, R. Binder, S. W. Koch, S. T. Cundiff, H. Wang, and D. G. Steel, Phys. Rev. B **49**, 14 382 (1994).
[46] H. Wang, K. B. Ferrio, and D. G. Steel, Phys. Rev. A **49**, R1551 (1994).
[47] W. Schäfer, in *Optics of Semiconductor Nanostructures* (Akademie-Verlag, Berlin, 1993), p. 21.
[48] V. G. Lyssenko, J. Erland, I. Balslev, K.-H. Pantke, B. Raxbirin, and J. M. Hvam, Phys. Rev. B **48**, 5720 (1993).
[49] F. H. Pollak and M. Cardona, Phys. Rev. **172**, 816 (1968).
[50] O. Kinrot and Y. Prior, Phys. Rev. A **50**, R1999 (1994).
[51] H. J. Bakker and H. Kurz, Phys. Rev. B **50**, 7805 (1994).
[52] W. Schäfer, D. S. Kim, J. Shah, T. C.Damen, J. E. Cunningham, K. W. Goossen, L. N. Pfeiffer, and K. Köler, Phys. Rev. B **53**, 16 429 (1996).
[53] M. Koch, J. Feldmann, G. von Plessen, and E. O. Göbel, Phys. Rev. Lett. **69**, 3631 (1992).
[54] This approximation scheme has also been called the ''dynamics controlled truncation scheme.'' We prefer the specification ''coherently controlled truncation scheme,'' as the truncation results from a classification with respect to the power of external laser fields and not from the dynamics of the particle system.
[55] I. Balslev and E. Hanamura, Solid State Commun. **72**, 843 (1989).
[56] V. M. Axt and A. Stahl, Z. Phys. B **93**, 195 (1994).
[57] V. M. Axt, G. Bartels, and A. Stahl, Phys. Rev. Lett. **76**, 2543 (1996).
[58] K. Bott, O. Heller, D. Bennhardt, S. T. Cundiff, P. Thomas, E. J. Mayer, G. O. Smith, R. Eccleston, J. Kuhl, and K. Ploog, Phys. Rev. B **48**, 17 418 (1993).
[59] V. M. Axt, K. Victor, and T. Kuhn, Phys. Status Solidi B **206**, 189 (1998).
[60] H. Zhou, A. V. Nurmikko, C.-C. Chu, J. H. R. L. Gunshor, and T. Takagahara, Phys. Rev. B **58**, R10 131 (1998).
[61] W. Schäfer, I. Brener, and W. Knox, in *Coherent Optical Interactions in Semiconductors*, edited by R. T. Philipps (Plenum Press, New York, 1994), p. 343.
[62] M. Kira, F. Jahnke, and S. W. Koch, Phys. Rev. Lett. **81**, 3263 (1998).
[63] G. Bartels, A. Stahl, V. M. Axt, B. Haase, U. Neukirch, and J. Gutowski, Phys. Rev. Lett. **81**, 5880 (1998).
[64] H. Haug and S. Schmitt-Rink, Prog. Quantum Electron. **9**, 3 (1984).
[65] M. U. Wehner, J. Hetzler, and M. Wegener, Phys. Rev. B **55**, 4031 (1997).
[66] L. Schultheis, J. Kuhl, A. Honold, and C. W. Tu, Phys. Rev. Lett. **57**, 1635 (1986).
[67] L. Schultheis, J. Kuhl, A. Honold, and C. W. Tu, Phys. Rev. Lett. **57**, 1797 (1986).